Quaternary Science Reviews 392 (2026) 110261

Contents lists available at ScienceDirect

Quaternary Science Reviews

journal homepage: www.elsevier.com/locate/quascirev

New chronologies for the Middle Pleistocene formations within the southern North Sea

Michael J. Grant [a,*], Phillip Toms [b], Sally Evans [c], Jamie Wood [b], Alexander Smith [d,e], Matt Law [f], Justin K. Dix [g], Chris Walker [h], Tom Hill [i,g], Christin Heamagi [j]

[a] Coastal and Offshore Archaeological Research Services, School of Ocean and Earth Science, National Oceanography Centre Southampton, University of Southampton Waterfront Campus, European Way, Southampton, UK
[b] Luminescence Dating Laboratory, School of Education & Science, University of Gloucestershire, Swindon Road, Cheltenham, UK
[c] MSDS Marine, Holbrook, Belper, UK
[d] Ørsted, 5 Howick Place, Westminster, London, UK
[e] Present Address: TGS, 4 The Heights, Brooklands, Weybridge, Surrey, UK
[f] School of Sciences, Bath Spa University, Bath, UK
[g] School of Ocean and Earth Science, National Oceanography Centre Southampton, University of Southampton Waterfront Campus, European Way, Southampton, UK
[h] Fugro GB Limited, Fugro House, Hithercroft Rd, Wallingford, UK
[i] PalaeoEnvironmental Research and Consultancy Services (PERCS), Princes Risborough, UK
[j] Maritime Archaeology Ltd, National Oceanography Centre, Empress Dock, Southampton, UK

ARTICLE INFO

Handling Editor: Carin Andersson Dahl

ABSTRACT

There are few reliable chronological controls for the Middle Pleistocene Formations of the southern North Sea. Offshore Wind Farm developments in this area are providing unparalleled opportunities to map and investigate these deposits, revealing greater complexity than expected. Geotechnical site investigations offer new opportunities to apply scientific dating techniques to establish the absolute chronology of these deposits, rather than relying on traditional biostratigraphic approaches. This paper presents the results of investigations associated with the Hornsea One and Two Offshore Wind Farms, focusing on Middle to early Late Pleistocene Formations within the Inner Silver and Sole Pits. A new protocol for core handling procedures, implemented during geotechnical site investigations, increased access to core material suitable for paired luminescence dating (quartz OSL and K-feldspar pIRIR). The new dates demonstrate that the base of the Sand Hole Formation is late MIS 12 to MIS 11, with the Egmond Ground Formation likely accumulating through MIS 10 to 8. A deposit above the Egmond Ground Formation is shown to be chronologically, lithologically and biostratigraphically equivalent to the Brown Bank Formation, traditionally found only in the eastern southern North Sea and securely dated to late MIS 5a/early MIS 4. The new absolute dates provide much-needed clarity on the age of Middle Pleistocene Formations in this region and support revision of the existing chronostratigraphy for the southern North Sea.

1. Introduction

The Quaternary geology of much of the southern North Sea is Early to Middle Pleistocene in age, reflecting deposition in shallow-water, distal and deltaic environments (Cameron et al., 1992). However, most Quaternary and archaeological studies within the area, such as BRITICE (Clark et al., 2022; Dove et al., 2017) and the North Sea Palaeolandscape Project (Gaffney et al., 2007, Gaffney et al., 2009; Gaffney and Fitch, 2022), have understandably focused on the near-seabed, Late Pleistocene to Early Holocene record associated with the Devensian (Weichselian) glaciation and marine transgression phases. This has significantly increased our understanding of the timing of Late Pleistocene and Holocene events. However, the ages of many underlying Middle Pleistocene Formations remain poorly constrained, largely based on biostratigraphy and now-outdated glacial-interglacial frameworks (e.g., Mitchell et al., 1973), such as those adopted by Cameron et al. (1992), Tappin et al. (2011) and Stoker et al. (2011). Attempts to update this framework using data acquired during offshore wind farm developments continue to be hampered by very limited absolute-age constraints on sediments predating marine isotope stage

* Corresponding author.
E-mail address: M.J.Grant@soton.ac.uk (M.J. Grant).

https://doi.org/10.1016/j.quascirev.2026.110261
Received 28 November 2025; Received in revised form 2 September 2026; Accepted 2 September 2026
Available online 13 September 2026
0277-3791/© 2026 The Authors. Published by Elsevier Ltd. This is an open access article under the CC BY license (http://creativecommons.org/licenses/by/4.0/).

(MIS) 2 (Dakin et al., 2026).

This knowledge gap is due in part to two factors. One is accessibility: these deposits are often present at depth beneath the seabed (beyond the reach of conventional vibrocores), requiring sedimentary sampling techniques that are both logistically and financially more challenging for academics to access; the second is the availability of suitable material and techniques for dating these deposits. The latter is, in part, due to the applicable timespans of commonly used scientific dating techniques. Radiocarbon dating has a detection limit of c. 55 ka (Reimer et al., 2020), whereas Duller (2025) states that Optically Stimulated Luminescence (OSL) on quartz can commonly date to 100 ka, usually reaches 200 ka, and, only under optimal conditions, can reach ages of 400 to 600 ka (e.g. Pawley et al., 2010).

OSL has become a dominant scientific dating technique in large part because the rapid bleaching of the fast component of the quartz luminescence signal (Wintle and Murray, 2006), which minimises the likelihood of partial bleaching, is coupled with the apparent absence of anomalous fading commonly observed during Infrared stimulated luminescence (IRSL) of feldspars (Huntley and Lamothe, 2001). The widespread adoption of OSL has significantly improved the chronology of deposits within later Middle Pleistocene and Late Pleistocene sequences (post c. 300 ka). However, unless working in an area with average background radioactivity, the quartz OSL signal saturates after 150 ka years of burial or younger (Mahan and DeWitt, 2019), rendering this technique useless for many Middle Pleistocene sequences.

IRSL of feldspar saturates at a higher dose than quartz, providing the potential to extend the dating limit earlier into the Middle Pleistocene (e.g. Buylaert et al., 2007; Gibbard et al., 2021). Like quartz, feldspars are widely abundant and found in a variety of sedimentary settings, and, unlike quartz crystals, can be selectively measured under infrared excitation (Huntley and Lamothe, 2001). IRSL signals are less variable from region to region, and potassium-rich feldspar ('K-feldspar') grains generally emit a detectable luminescence signal that is brighter than that from quartz grains (Duller et al., 2003). However, IRSL dating of feldspar has been hampered by anomalous fading of the IRSL signal, leading to age underestimation. To overcome this issue, the post-IR IRSL (pIRIR) signal of K-feldspar, stimulated at a higher temperature after a prior low-temperature IR stimulation, exhibits a negligible fading rate (Thomsen et al., 2008; Zhang and Li, 2020), enabling successful dating applications. pIRIR therefore offers the opportunity to date Middle Pleistocene deposits that are at, or beyond, the limits of OSL. Combining quartz OSL and K-feldspar pIRIR (referred to as 'paired luminescence dating') provides additional benefits for securing robust scientific dating through a multi-dating approach (e.g. Yoon et al., 2022; Roberts et al., 2015). When dates agree, this can increase confidence in the deposit's age. Where discrepancies occur, this permits further consideration of the dating and sample taphonomy. Possible causes of discrepancy could be that the K-feldspar component was not bleached by sunlight at the time of deposition, as the pIRIR signal is less light-sensitive than the OSL signal (e.g. Roberts et al., 2015; Cheng et al., 2022; Zhang et al., 2023; Calarossi et al., 2015), or the quartz OSL signal is saturating and therefore only providing a terminus ante quem (TAQ).

The expansion of offshore wind capacity worldwide, largely driven by the desire for energy transition and to meet net-zero goals, has created many opportunities to better understand Quaternary geology in the marine zone. For the developer, this is largely driven by the need to build ground models to inform site design and geohazard assessment, achieved through the collection of marine geophysical and geotechnical datasets. This has been particularly relevant in the southern North Sea, where new site investigations have provided high-resolution mapping of the subsurface geology, aided by the development and application of Ultra High Resolution (UHR) seismic surveys (Caselitz et al., 2025) and extensive geotechnical site investigations. Ground model development has revealed a more complex Quaternary geology than originally anticipated (e.g., Arlott et al., 2023; Cotterill et al., 2017). These datasets have also enabled the identification of submerged palaeolandscapes, which form part of the historic environment as defined in the UK Marine Policy Statement (2011) and may therefore be affected by offshore development (Firth, 2013; Jones and Salter, 2017; Sturt et al., 2017). Developer-led geotechnical site investigations therefore provide valuable opportunities to access, characterise and date Quaternary deposits, permitting testing and refinement of the existing chronology of the Middle Pleistocene formations.

In this paper, we present the results of site investigations undertaken to support the Hornsea Two Offshore Wind Farm (HOW02) and demonstrate how the adoption of quartz OSL and K-feldspar pIRIR dating, coupled with traditional biostratigraphic techniques, has provided a new chronology for Middle Pleistocene formations encountered along the export cable corridor (ECC). Running parallel to the HOW02 ECC is the Hornsea One Offshore Wind Farm (HOW01) ECC. Datasets collected for the HOW01 ECC are also considered in this paper, including a reassessment of the results of geoarchaeological investigations in the Inner Silver Pit area (Heamagi, 2018).

2. Study area

HOW01 and HOW02 are located within a group of Ørsted windfarm projects in the southern North Sea (Fig. 1). The HOW02 site is located approximately 90 km east of the English coast, with a wind turbine generation (WTG) capacity of 1.32 GW, which went operational in August 2022, making it the largest wind farm in the world at that time. The WTG area covers 462 km^2 and shares a common border with HOW01, located immediately to the south and east. The northern limit of HOW02 is defined by the southern edge of the Outer Silver Pit — a large, elongated seabed depression measuring >100 m deep. HOW01 and HOW02 are connected to the UK Energy grid through a 115 km ECC making landfall at Horseshoe Point, North Lincolnshire, within the Outer Humber Estuary (see Grant et al., 2024).

The majority of the ECC is underlain by Upper Cretaceous Chalk, which deepens eastwards. 24 km east of the Inner Silver Pit, the chalk disappears, revealing the underlying Jurassic geology, consisting of mudstones and limestones of the Humber Group (Upper Jurassic), sandstones and mudstones of the West Sole Group (Middle Jurassic), and mudstones and limestones of the Lias Group (Lower Jurassic). These continue eastwards until the Well Bank Flat area, where the WTGs are located, and the Jurassic geology is unconformably overlain by Eocene mudstones and sandstones (see Cameron et al., 1992).

Overlying the solid geology are Quaternary deposits (Table 1). Along most of the ECC, the Bolders Bank Formation occurs at or near the seabed surface. This is interpreted as a Devensian ablation till, forming a Broad Sediment Wedge (BSW) delineated to the south by a series of east-west, discontinuous ridge-chains across the seabed, which are glacial landforms (e.g. moraines) associated with Devensian ice-sheet margins (shown in Fig. 1; see Dove et al., 2017; Roberts et al., 2018).

The ECC crosses two notable offshore deeps along the route; the Inner Silver Pit (ISP; deepening to −75 m LAT) and the Sole Pit (SP; deepening to −50 m LAT). These deeps have been interpreted as subglacial tunnel valleys (Ehlers and Wingfield, 1991), exhibiting U-shaped cross-sectional and scoop-shaped longitudinal profiles with reverse slopes at both the northern and southern ends. The orientation of these deeps is roughly perpendicular to the local orientation of the Bolders Bank Formation BSW (Dove et al., 2017). Erosion of the tunnel valleys down to the underlying geology has led to the near-surface exposure of Middle Pleistocene deposits at their margins, allowing them to be sampled using shallow (6m long) vibrocores.

3. Methodology

3.1. Geophysical survey

Geophysical surveys along the ECC were conducted during multiple campaigns by Bibby Hydromap, Gardline Geosurvey and Fugro (see Supplementary Material S1). Most surveys used a hull-mounted Pinger,

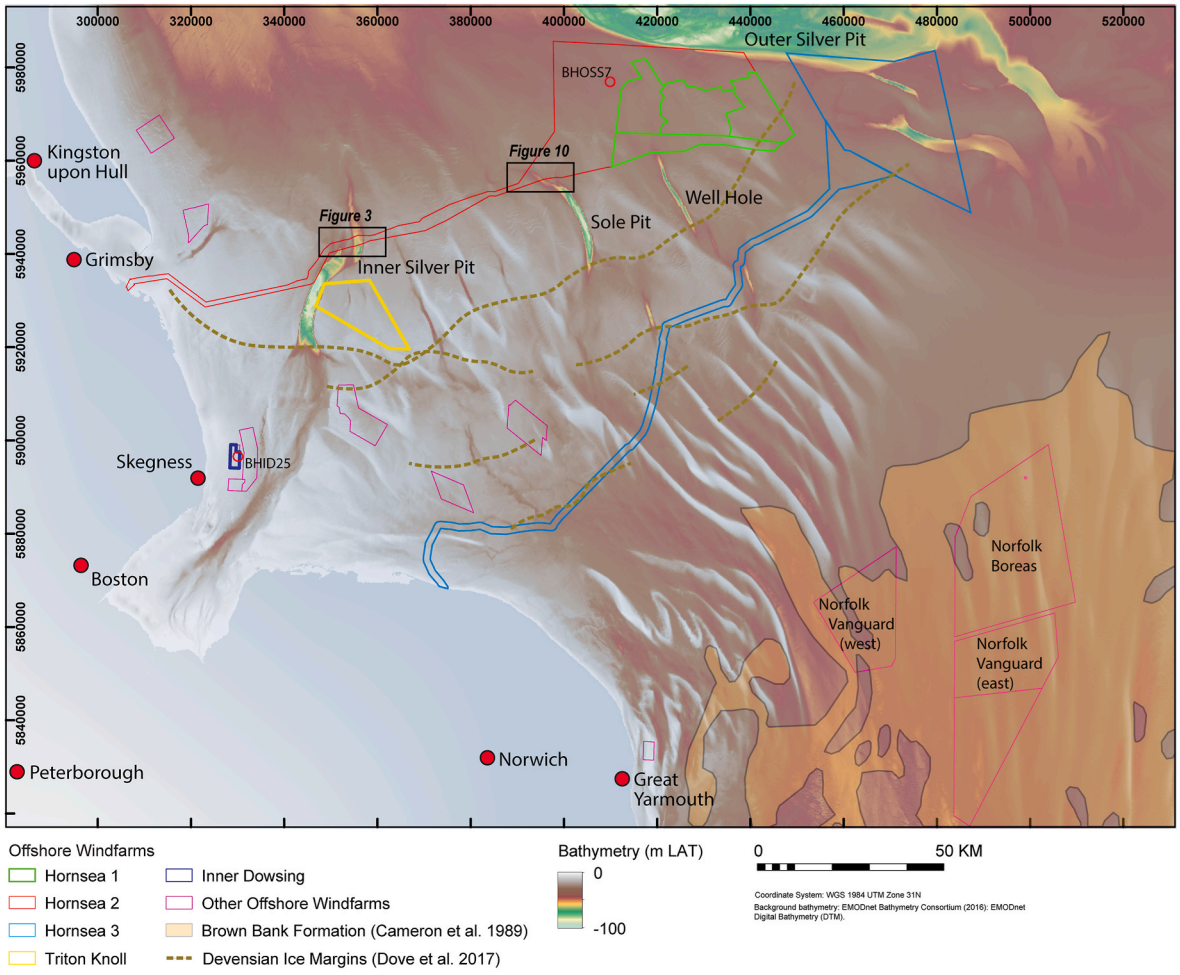


Fig. 1. Bathymetric map of the southern North Sea including wind farm zones, sites/cores referred to in the text, Devensian (MIS 2) ice margins (Dove et al., 2017) and the known extent of the Brown Bank Formation, as mapped by Cameron et al., 1992).

though additional lines were also collected using a Geo Source Cat Sparker. Survey lines were typically aligned parallel to the ECC, and the multiple surveys have resulted in significant overlap, producing dense line spacing, sometimes as little as 5-20 m apart. A conversion from two-way travel time (TWT) to depth (m) was applied using a sound velocity of 1480 m/s in water and 1600 m/s in sediments. Multibeam bathymetry survey data were tidally corrected to Lowest Astronomical Tide (LAT).

3.2. Core handling procedures

Luminescence dating requires shielding of the sediment being analysed from light. This is typically achieved for marine sediment cores using opaque core liners and sampling under controlled laboratory conditions (Duller, 2008). However, this approach is not always possible or practical, especially when samples are collected for geotechnical purposes. Alternative procedures are therefore required to ensure that luminescence dating remains achievable (e.g. Tappin et al., 2011; Bynoe et al., 2022). For HOW02, a protocol was developed in conjunction with the geotechnical survey contractor, Fugro GB; the developer, Ørsted; and the retained archaeologist, MSDS Marine, to provide guidance on the identification, extraction, storage and transport of marine sediment cores to ensure the availability of samples suitable for luminescence dating (MSDS Marine, 2018). This method statement was also agreed with the Historic England Marine Planning Unit prior to mobilisation. The procedures adopted are summarised in Fig. 2.

Vibrocores were collected by Fugro Marine Limited along the ECC in 2018 aboard the *MV Despina* using Fugro's High Performance Corer. Core splitting commenced in July 2018, following a toolbox talk at Fugro's facilities in Wallingford, Oxfordshire. The toolbox talk allowed the retained geoarchaeologist to explain the proposed sampling protocol to the ship- and laboratory-based geotechnical teams, discuss any modifications to existing core-handling procedures, outline the key deposit types, and establish lines of communication. This enabled laboratory staff to recognise deposits with high potential at an earlier stage and to seek advice at the earliest opportunity.

Cores were split longitudinally using a core splitter, with the split sections carefully divided using a knife or steel string. One exposed section was then recorded and photographed, ensuring that the exposed surface of the split-core section was not disturbed, thereby keeping the underlying sediments light-shielded. Cores were then wrapped in clear and opaque polythene to prevent further light exposure, and the core logs and photographs were provided to the geoarchaeological specialist to make recommendations prior to any further core sampling (see Fig. 2).

Seven vibrocores were taken across the ISP, with four taken across the SP (see Fig. 3 and Fig. 10). Following the assessment of each core record, together with the sub-bottom geophysical datasets, two cores from each of these deeps were selected for further investigation (Table 2).

The selected cores underwent geoarchaeological assessment in accordance with the guidelines from Historic England (2015) and Gribble and Leather (2011), with sediment descriptions following Hodgson (1997). Photographs and core descriptions are provided in Supplementary Material S2.

Table 1
Summary of the Quaternary stratigraphy and assigned chronology of the Inner Silver Pit and Sole Pit sequences.

Formation (Cameron et al., 1992/ Ansari, 1992/(Dakin et al., 2026))	Formation (Arlott et al., 2023: Triton Knoll Offshore Wind Farm)	Seismic Unit in this Study	Expected Sediments	Chronology
Southern Bight	Holocene Marine Sands	ISP-9 SP-5	Very loose to very dense sand with gravel and shell fragments or very soft to firm clay	MIS 1
Elbow	Not reported	Not present	Muddy sand, interbedded clay and peat	MIS 1
Botney Cut	Botney Cut	ISP-8[a]	Interbedded loose to very sense sand and very soft to very stiff clay locally with a bed of gravel	MIS 2 to early MIS 1
Bolders Bank	Bolders Bank	ISP-7 SP-4	Firm to very stiff becoming hard clay with gravel, shell fragments and laminations, beds and pockets of silt and medium sense to very dense sand	MIS 3-2
Brown Bank	Not reported	ISP-6	Silty sand and sandy silt	MIS 5b-4[b]
Eem	Not reported	?upper ISP-5	Shelly sands; can be muddy in places	MIS 5e-b
Egmond Ground	Egmond Ground	ISP-5 SP-3 SP-2	Interbedded medium dense to very dense sand and very stiff to hard clay	MIS 10-8[b] possibly as late as MIS 6
	Upper Sand Hole Formation (USHF)	ISP-4	Medium to very dense sand and very high strength clay with varying thickness	Possibly MIS 10/9[b]
Sand Hole	Lower Sand Hole Formation (LSHF)	ISP-3	High strength clay with occasional beds of sand	Late MIS 12 to early MIS 10
Swarte Bank	Swarte Bank	ISP-2	Interbedded to interlaminated very stiff to very hard clay and medium dense to dense sand	MIS 12
Underlying Geology				
Cretaceous Chalk	Chalk	ISP-1		
Jurassic Lias Group	Not reported	SP-1		

[a] Botney Cut Formation was only observed beyond the boundaries of the two Pits.
[b] Updated chronology based upon the result from this study and 'Waajen-Labee et al. (2025).

3.3. Luminescence dating

The choice of sampling position for luminescence dating was informed by sedimentological descriptions, chronological questions posed during the geoarchaeological assessment, and considerations of texture and visible core integrity. Sampled units needed to be at least 100 mm thick, with a retained sample length of at least 300 mm, to ensure sufficient light-shielding, reduce contamination (e.g., proximity to the ends of cores, visible cracks in samples, etc.), and allow assessment of sample homogeneity during luminescence sampling under controlled laboratory illumination. Units with visible cracks and/or comprising material that lacks cohesion to survive sampling and/or transport in normal lighting conditions were avoided.

Core sections identified as suitable for luminescence dating were transported to the Luminescence Dating Laboratory, University of Gloucestershire, where sub-sampling under controlled laboratory illumination (using Encapsulite RB-10 (red) filters) was carried out. To isolate material that may have been exposed to daylight during sampling, sediment within 10 mm of each core face was removed.

The remaining sample was dried and then sieved, with the fine-sand fraction segregated and subjected to acid and alkaline digestion (10% HCl, 15% H_2O_2) to attain removal of carbonate and organic components, respectively. The sample was then divided into two. For one half, a further acid digestion in HF (40%, 60 min) was used to etch the outer 10-15 μm layer affected by α radiation and degrade each sample's feldspar content. During HF treatment, continuous magnetic stirring was used to effect isotropic etching of grains. 10% HCl was then added to remove acid-soluble fluorides. Each sample was dried, re-sieved, and quartz isolated from the remaining heavy mineral fraction using a sodium polytungstate density separation at 2.68 g cm^{-3}. For the second half, density separations at 2.53 and 2.58 g cm^{-3} were undertaken to isolate the K-feldspar fraction. Twelve 8 mm multi-grain aliquots (~4 mg) of quartz and K-feldspar were then mounted on aluminium discs for determination of D_e values.

Equivalent dose (D_e) values were quantified using a single-aliquot regenerative-dose (SAR) protocol (Murray and Wintle, 2000, 2003 for quartz; Li et al., 2014 for K-feldspar). For quartz, this was facilitated by a Freiberg Instruments Lexsyg Smart irradiation-stimulation-detection system (Richter et al., 2015). Within this apparatus, optical signal stimulation is provided by an assembly of blue laser diodes, filtered to 445 ± 3 nm conveying 30 mW cm^{-2} using a 3 mm Schott GG420 and HC448/20 positioned in front of each laser diode, with aliquots held at ~125°C (105°C substrate temperature). Infrared (IR) stimulation, provided by IR laser diodes stimulating at 850 ± 3 nm filtered by 3 mm RG 715 and delivering ~200 mW cm^{-2}, was used to indicate the presence of contaminant feldspars (Hütt et al., 1988). Stimulated photon emissions from quartz aliquots are in the ultraviolet (UV) range. These were divided from stimulating photons by 2.5 mm Hoya U-340 and 1 mm NG4 glass filters, and a Delta BP 365/50 interference filter, then detected by a Hamamatsu UV-VIS (300-650 nm) bi-alkaline cathode photomultiplier. K-feldspar D_e values were acquired using a Risø TL-DA-15 irradiation--stimulation-detection system (Markey et al., 1997; Bøtter-Jensen et al., 1999). Optical signal stimulation was provided by an assembly of blue diodes, filtered to 445 ± 3 nm conveying 30 mW cm^{-2} using a 3 mm Schott GG420 and HC448/20 positioned in front of each diode pack. Infrared (IR) stimulation for K-feldspars was provided by 6 IR diodes (Telefunken TSHA 6203) stimulating at 875 ± 80 nm delivering ~40 mW cm^{-2}; power was reduced to ~12 mW cm^{-2} owing to the strength of the IRSL signal in these samples. IR stimulation was performed at 50°C then 200°C to remove the fading signal, with the non-fading signal then measured at 250°C (Li et al., 2014). K-feldspar emissions were filtered by 2 mm Schott BG-39 and 3 mm Schott BG-3 glass. Inter-cycle optical stimulation was conducted at 280°C for quartz and 320°C for K-feldspar to minimise recuperation.

For both minerals, aliquot irradiation was conducted using $^{90}Sr/^{90}Y$ β sources calibrated for fine sand, multi-grain aliquots against the 'Hotspot 800' ^{60}Co γ source located at the National Physical Laboratory (NPL), UK, delivering 0.11 Gy s^{-1} to quartz and 0.06 Gy s^{-1} to K-feldspar on the Lexsyg and Risø systems, respectively. OSL and pIRIR sensitivity change during measurement was monitored and corrected for using a 5 Gy test dose and 220°C, 10 s preheat for quartz and 30 Gy test dose and 300°C, 60 s preheat for K-feldspar.

The presence of feldspar contaminants within quartz was assessed using the post-IR OSL ratio (Duller, 2003). The choice of natural and regenerative-dose preheating was informed by Dose Recovery tests

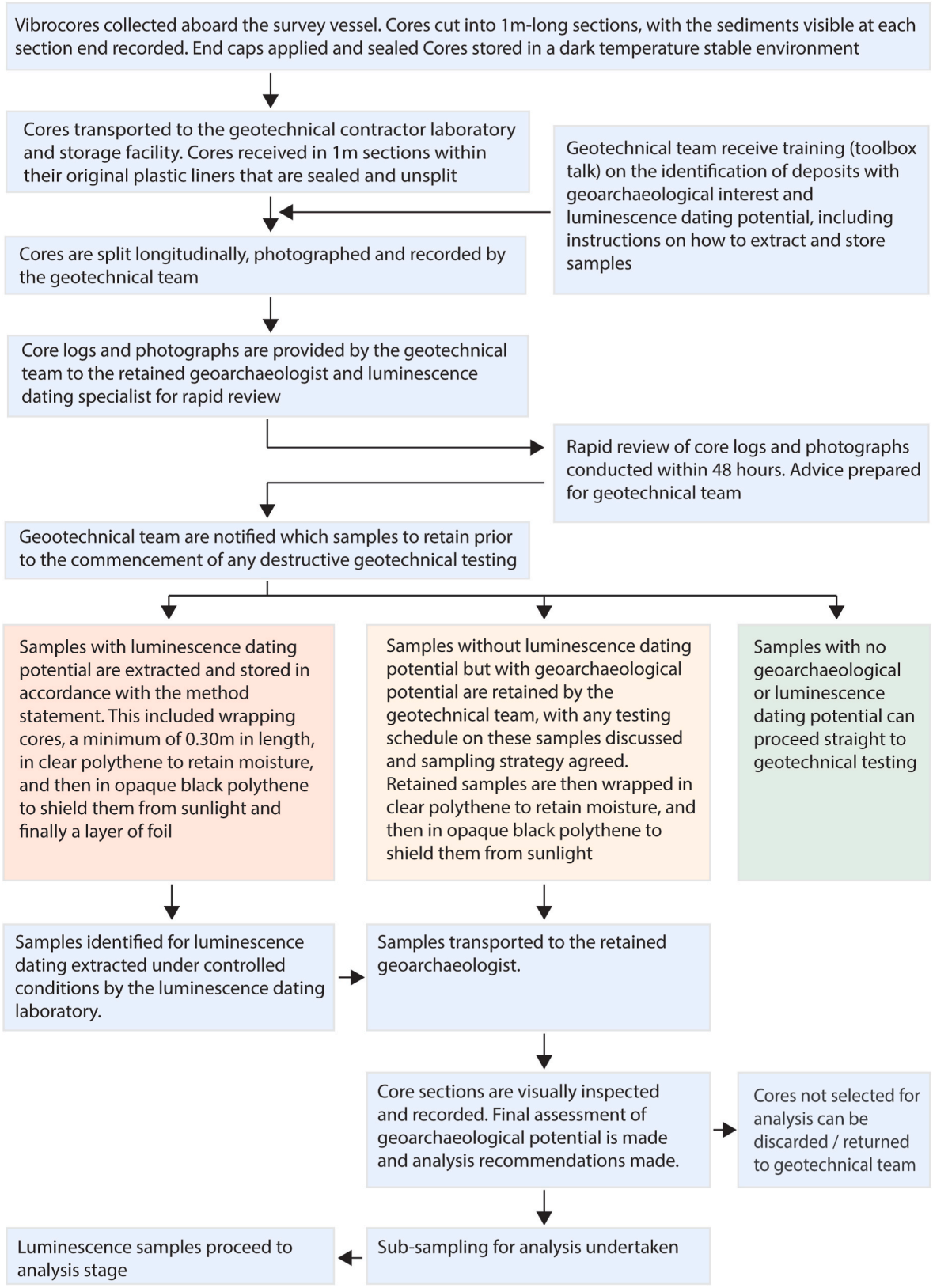


Fig. 2. Summary of core handling procedures.

(Murray and Wintle, 2003). For quartz, 6 aliquots were each assigned a 10 s preheat between 180°C and 280°C. For the K-feldspar fraction, the efficacy of the 300°C, 60 s preheat in Dose Recovery was assessed from the average of three aliquots. The success of regenerative-dose sensitivity correction was monitored using both low- and high-dose recycling ratios (Murray and Wintle, 2000).

D_e values were interpolated from regenerative dose response curves, fitted with an exponential plus linear regression, using Analyst (Duller,

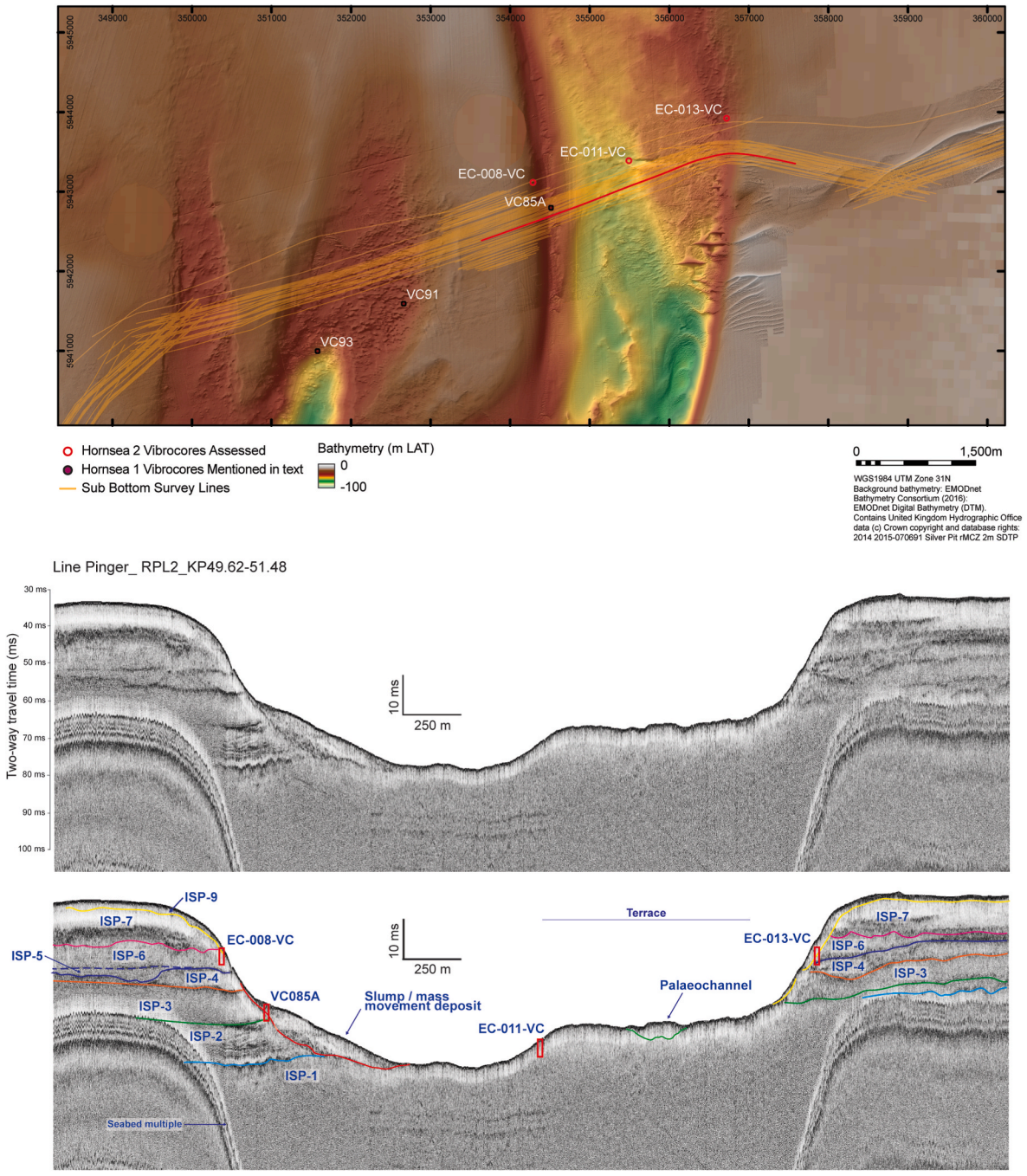


Fig. 3. Geophysical profile across the Inner Silver Pit, showing the interpreted Pleistocene stratigraphy and the relative positions of the cores mentioned in the main text. See Table 1 for a summary of Quaternary Formations.

2015). Weighted (geometric) mean D_e values were calculated using the central age model outlined by Galbraith et al. (1999).

For lithogenic radiation external to the grains of quartz and K-feldspar, dose rate (D_r) values were defined through measurement of U, Th and K radionuclide concentration and conversion of these quantities into β, γ and, for K-feldspar, α D_r values. Radionuclide concentrations were estimated from sub-samples by laboratory-based γ-spectrometry using an Ortec GEM-S high-purity Ge coaxial detector system, calibrated using certified reference materials supplied by CANMET. The level of U disequilibrium was estimated by laboratory-based Ge γ spectrometry. Estimates of radionuclide concentration were converted to D_r values (Adamiec and Aitken, 1998), accounting for D_r modulation forced by grain size (Mejdahl, 1979) and present moisture content (Zimmerman, 1971).

Lithogenic radiation internal to K-feldspar grains was assumed to be derived from a K content of 12.5%. Cosmogenic D_r values were calculated based on sample depth, geographic position, and matrix density (Prescott and Hutton, 1994).

Luminescence dating results (Table 3 and Table 4) provide an estimate of the sediment burial period based on mean D_e and D_r values and their associated analytical uncertainties. Dates are quoted as years before AD 2000 (b2k). Further details are provided in Supplementary Material S3. Several dates have associated considerations, listed in Table 4.

For the dated sequences from EC-008-VC, EC-011-VC and EC-023-VC, a Sequence Model was constructed in OxCal 4.4.4 (Bronk Ramsey, 2009, 2021). The Sequence function was selected because, although the stratigraphic order of the dates is known for each sequence, the

Table 2
Vibrocores from the Inner Silver and Sole Pits subject to analysis. Locations shown in Figs. 3 and 10.

Vibrocore	Easting (WGS84 UTM31N)	Northing (WGS84 UTM31N)	Seabed elevation (m LAT)	Core length	Location
EC-008-VC	354286	5943119	−32.90	6.00m	Inner Silver Pit western margin
EC-011-VC	355493	5943394	−60.90	6.00m	Inner Silver Pit base
EC-022-VC	393247	5957168	−45.80	5.85m	Sole Pit base
EC-023-VC	393509	5957350	−39.20	6.40m	Sole Pit eastern margin

deposition rate and potential gaps between dates are unknown and may not be suitable for a P-sequence. The posterior density estimates from the Bayesian chronological modelling are provided in Table 4.

3.4. Pollen

Standard preparation procedures were used (Moore et al., 1991). 2 cm^3 of sediment was processed from each sample.

Pollen counting was conducted at 400× magnification using a Nikon Eclipse Ci-L transmitted-light microscope. Determinable pollen and spore types were identified to the lowest possible taxonomic level, with reference to a collection held at COARS, University of Southampton. Pollen and spore types follow Bennett (1994; Bennett et al., 1994), except for Poaceae (Küster, 1988), Cupressaceae (Moore et al., 1991), Azollaceae (Stafford, 2003), and Betulaceae (Blackmore et al., 2003). Plant nomenclature follows Stace (2010). The pollen assemblage was expressed as % total land pollen (TLP). The TLP sum excludes aquatics and pteridophytes, which are reported as % + Group. A minimum TLP sum of 200 TLP was recorded for samples from EC-008-VC, with counts exceeding 400 TLP for samples from EC-011-VC and EC-023-VC.

3.5. Diatoms

Diatoms were absent from all samples assessed. A number of factors could explain their absence. For example, iron oxide precipitation was often visible in some samples during slide assessment, which can be responsible for the dissolution of the biogenic silica that makes up the diatom frustule (Mayer et al., 1991). Scourse et al. (1998) also observed a lack of diatom preservation during their examination of the Swarte Bank and Sand Hole Formations in the ISP area, although Cameron (2018) recovered a small assemblage from VC091.

3.6. Foraminifera and molluscs

Foraminifera and molluscan analyses followed guidance set out by Historic England (2011). For foraminifera, samples were weighed, washed through a 63 μm mesh sieve, and air-dried before being sorted into fractions using a nest of sieves (4 mm, 2 mm, 1 mm, 500 μm, 250 μm, 125 μm, 63 μm). Biological remains were identified using a low-power binocular microscope and a reference collection. Ecological information for mollusca is derived from Allcock et al. (2017) and Graham (1971), and for foraminifera from Murray (1973, 1979, 1991, 2006). Nomenclature follows the WoRMS Editorial Board (2025). To aid interpretation, foraminifera and molluscs are grouped into broad ecological groups that correspond to their habitat preferences.

4. Results

4.1. Inner Silver pit crossing

Interpretation of the seismostratigraphy has been aided by comparison with results from the Triton Knoll Offshore Windfarm development (~8 km south; Gardline, 2015; Arlott et al., 2023). The Quaternary formations present are summarised in Table 1 and discussed below, divided into nine stratigraphic units. An example seismic profile across the ISP is shown in Fig. 3.

A basal Quaternary seismic unit, ISP-2, containing high-amplitude horizontal and dipping reflectors, overlies the chalk surface (ISP-1) on the western side of the ISP. It measures 7.7 m (9.6 ms TWT) in vertical thickness and is traceable 5 km westwards, where it thickens to ~13.2 m (16.5 ms TWT). Traces of this unit may also be visible to the east of the ISP, where it reaches a maximum thickness of ~2.2 m (2.8 ms TWT). ISP-2 is attributed to the Swarte Bank Formation.

On both sides of the deep, overlying the Swarte Bank Formation/chalk surface, an acoustically transparent seismic unit (ISP-3) with weakly developed horizontal internal reflectors is present. This unit thickens to a maximum of 12 m (15 ms TWT) 5 km west of the ISP. During the HOW01 site investigations, the base of this unit was sampled at VC085A, recorded as a "stiff, high strength dark grey (2.5Y 4/1) slightly sandy, silty clay with abundant extremely closely spaced shelly fine sand partings" (Fugro, 2013). Following the scheme of Arlott et al. (2023), ISP-3 is correlated with the Lower Sand Hole Formation (LSHF). Overlying this, a complex seismic unit, ISP-4, contains many undulating, incising and cross-bedded reflectors. ISP-4 is correlated with the Upper Sand Hole Formation (USHF) identified by Arlott et al. (2023; their Unit B facies), which they interpreted as a complex depositional environment comprising both filled channels and buried dunes. This revises the earlier interpretation by Ansari (1992) that this seismic unit was part of the Egmond Ground Formation. This seismic unit can only be traced ~800 m west and ~500 m east of the ISP.

Above ISP-4 lies another acoustically transparent to weakly horizontally bedded seismic unit. ISP-4 is correlated with the Egmond Ground Formation of Cameron et al. (1992). ISP-4 is poorly defined in the northern part of the ISP, with apparent thickening to the south, as seen at the Triton Knoll OWF (Arlott et al., 2023; Ansari, 1992). Separating the Egmond Ground and later Eem Formations acoustically is challenging, often leading to their collective designation as the Egmond Ground Formation (Cameron et al., 1992) because the separating reflector is poorly defined. To the west of the ISP, an internal reflector may separate these two formations, but no such reflector can be identified to the east. No core samples were available from this area to assess whether this might be the Eem Formation.

Where identified, the undulating ISP-4 surface is infilled and overlain by a strong basal reflector, above which lies a higher-amplitude, horizontally bedded seismic unit, ISP-6. Cores EC-008-VC and EC-013-VC, taken through the upper slopes on either side of the ISP, confirm the presence of a horizontally laminated clayey loam associated with ISP-6. Although this seismic unit might traditionally be assigned to the Eem Formation, the nature of the sediments and their age, as discussed below, make it more likely that it is equivalent to the Brown Bank Formation, which is traditionally reported to consist of medium-to high-amplitude subparallel internal reflections bounded by high-amplitude lower and upper bounding reflections (Waajen-Labee et al., 2025).

Lateral tracing of ISP-6 westwards shows that it is present near the surface in the shallower deeps, as confirmed in VC091 and VC093 by the presence of the same horizontally laminated clayey loam. This seismic unit was originally interpreted by Wessex Archaeology (2013) as the Botney Cut Formation, though the seismic profiles clearly show that this deposit extends laterally beneath ISP-7 (Bolders Bank Formation; see below) and is traceable to the edge of the ISP, where EC-008-VC was collected from ISP-6. Radiocarbon dates from this laminated deposit in VC091 (Table 5; Heamagi, 2018) confirm that ISP-6 pre-dates the

Table 3
Luminescence Dating: underpinning Dr and De data for samples. Sample locations shown in Fig. 4.

Lab Code	Seismic Unit	Core	Depth (m)	Mineral	Moisture content (%)	Ge γ-spectrometry (ex situ)			Internal β D_r (Gy ka^{-1})	External α D_r (Gy ka^{-1})	External β D_r (Gy ka^{-1})	External γ D_r (Gy ka^{-1})	Cosmic D_r (Gy ka^{-1})	Low Dose Recycling Ratio	High Dose Recycling Ratio	Post-IR OSL Ratio
						K (%)	Th (ppm)	U (ppm)								
GL20004	ISP-6	EC-008-VC	3.25	Quartz K-feldspar	17	1.32 ± 0.10	3.45 ± 0.36	0.76 ± 0.12	- 0.53 ± 0.10	- 0.09 ± 0.03	0.91 ± 0.12	0.46 ± 0.09	0.12 ± 0.01	0.91 ± 0.06 0.96 ± 0.03	1.01 ± 0.06 1.02 ± 0.03	1.01 ± 0.07 -
GL20005	ISP-6	EC-008-VC	4.70	Quartz K-feldspar	17	1.21 ± 0.10	3.00 ± 0.36	0.74 ± 0.09	- 0.53 ± 0.10	- 0.08 ± 0.02	0.84 ± 0.11	0.42 ± 0.09	0.10 ± 0.01	0.94 ± 0.06 0.95 ± 0.02	1.03 ± 0.06 0.97 ± 0.02	1.00 ± 0.06 -
GL20006	ISP-6	EC-008-VC	5.43	Quartz K-feldspar	22	2.31 ± 0.15	10.81 ± 0.62	2.23 ± 0.15	- 0.64 ± 0.21	- 0.22 ± 0.08	1.79 ± 0.20 1.63 ± 0.21	1.00 ± 0.10 1.00 ± 0.15	0.09 ± 0.01	1.02 ± 0.04 1.00 ± 0.03	1.02 ± 0.04 0.99 ± 0.02	1.02 ± 0.05 -
GL20007	ISP-3	EC-011-VC	1.88	Quartz K-feldspar	14	0.87 ± 0.08	2.64 ± 0.31	0.58 ± 0.10	- 0.53 ± 0.10	- 0.07 ± 0.02	0.62 ± 0.09 0.64 ± 0.09	0.34 ± 0.07	0.15 ± 0.01	1.03 ± 0.04 0.98 ± 0.04	0.99 ± 0.06 0.99 ± 0.04	0.83 ± 0.06 -
GL20008	ISP-3	EC-011-VC	2.78	Quartz K-feldspar	12	0.81 ± 0.08	1.88 ± 0.30	0.39 ± 0.09	- 0.74 ± 0.12	- 0.04 ± 0.01	0.57 ± 0.08	0.28 ± 0.07	0.13 ± 0.01	1.01 ± 0.04 Insufficient material	0.97 ± 0.04 Insufficient material	0.82 ± 0.03 -
GL20009	ISP-3	EC-011-VC	3.75	Quartz K-feldspar	12	0.68 ± 0.07	2.24 ± 0.32	0.43 ± 0.09	- 0.74 ± 0.12	- 0.04 ± 0.01	0.52 ± 0.08 0.50 ± 0.07	0.28 ± 0.07	0.11 ± 0.01	1.00 ± 0.06 0.98 ± 0.03	1.03 ± 0.05 0.96 ± 0.03	0.78 ± 0.04 -
GL20012	SP-3	EC-022-VC	3.49	Quartz K-feldspar	19	0.53 ± 0.06	3.36 ± 0.36	0.78 ± 0.10	- 0.74 ± 0.12	- 0.06 ± 0.02	0.43 ± 0.07	0.30 ± 0.06	0.12 ± 0.01	0.99 ± 0.05 -	1.01 ± 0.05 -	0.97 ± 0.04 -
GL20013	SP-3	EC-022-VC	5.75	Quartz K-feldspar	16	0.50 ± 0.06	2.72 ± 0.35	1.89 ± 0.13	- 0.74 ± 0.12	- 0.10 ± 0.03	0.53 ± 0.07	0.38 ± 0.06	0.08 ± 0.01	1.10 ± 0.05 Insufficient material	1.00 ± 0.04 Insufficient material	0.93 ± 0.04 -
GL20014	SP-2	EC-023-VC	2.82	Quartz K-feldspar	18	1.60 ± 0.11	4.53 ± 0.39	0.83 ± 0.11	- 0.53 ± 0.10	- 0.11 ± 0.03	1.10 ± 0.14	0.56 ± 0.10	0.13 ± 0.01	1.04 ± 0.04 1.01 ± 0.05	1.02 ± 0.04 0.97 ± 0.04	0.94 ± 0.04 -
GL20015	SP-2	EC-023-VC	4.88	Quartz K-feldspar	17	1.39 ± 0.10	4.79 ± 0.42	1.07 ± 0.11	- 0.53 ± 0.10	- 0.12 ± 0.04	1.00 ± 0.13	0.55 ± 0.10	0.10 ± 0.01	1.02 ± 0.03 0.98 ± 0.04	0.98 ± 0.03 1.01 ± 0.04	0.82 ± 0.03 -
GL20016	SP-2	EC-023-VC	6.12	Quartz K-feldspar	19	2.15 ± 0.14	11.02 ± 0.64	2.10 ± 0.15	- 0.53 ± 0.10	- 0.26 ± 0.07	1.63 ± 0.20	1.02 ± 0.11	0.08 ± 0.01	1.04 ± 0.03 0.96 ± 0.04	1.02 ± 0.03 0.98 ± 0.04	0.94 ± 0.03 -

Table 4
Luminescence Dating: D_r, D_e, age data and analytical validity of samples. Age estimates are expressed relative to the year of sampling. Uncertainties in age are quoted at 1σ confidence, are based on analytical errors, and reflect combined systematic and experimental variability and (in parenthess) experimental variability alone. Modelled and unmodelled dates are provided at 2σ confidence, with ka indicating before AD 2000. Lab codes within the main text use the suffix 'Q' for quartz and 'F' for K-feldspar. Sample locations are shown in Fig. 4.

Lab Code	Core	Mineral	Total D_r (Gy ka^{-1})	D_e (Gy)	Age (ka) (68.3%)	Sample considerations	Unmodelled Date (ka b2k) (95%)	*Posterior Density Estimate* (ka b2k) (95%)	Seismic Unit
GL20004	EC-008-VC	Quartz	1.50 ± 0.14	109.6 ± 10.6	73.2 ± 10.0 (9.4)	None	81.0-61.1	*84.3-70.2*	ISP-6
		K-feldspar	2.11 ± 0.17	174.6 ± 7.1	82.8 ± 7.6 (6.7)				
GL20005	EC-008-VC	Quartz	1.36 ± 0.13	103.9 ± 7.6	76.7 ± 9.3 (8.4)	None	91.9-67.6	*82.7-69.0*	ISP-6
		K-feldspar	1.96 ± 0.16	160.9 ± 7.5	82.1 ± 7.9 (7.0)				
GL20006	EC-008-VC	Quartz	3.28 ± 0.23	236.4 ± 12.5	72.0 ± 6.3 (5.5)	None	91.4-67.0	*81.5-66.4*	ISP-6
		K-feldspar	3.59 ± 0.36	250.1 ± 13.6	69.7 ± 8.0 (7.4)				
GL20007	EC-011-VC	Quartz	1.11 ± 0.10	247.3 ± 33.9	222.7 ± 36.5 (34.8)	Significant feldspar contamination: accept as minimum age estimate	491.8-339.0	*474.8-343.0*	ISP-3
		K-feldspar	1.72 ± 0.14	715.3 ± 34.5	415.4 ± 38.2 (34.0)	None			
GL20008	EC-011-VC	Quartz	0.99 ± 0.09	197.5 ± 28.4	200.5 ± 34.3 (32.7)	Significant feldspar contamination: accept as minimum age estimate	N/A	*N/A*	ISP-3
		K-feldspar	1.76 ± 0.15	Insufficient datable material	-	Insufficient datable material			
GL20009	EC-011-VC	Quartz	0.90 ± 0.09	202.2 ± 30.4	223.5 ± 39.7 (38.1)	Significant feldspar contamination: accept as minimum age estimate	530.0-349.2	*520.2-378.3*	ISP-3
		K-feldspar	1.49 ± 0.13	734.1 ± 39.2	439.6 ± 45.2 (41.8)	None			
GL20012	EC-022-VC	Quartz	0.84 ± 0.08	435.5 ± 56.9	518.3 ± 84.7 (81.5)	D_e exceeds saturation threshold: accept as minimum age estimate	687.7-348.9	*N/A*	SP-3
		K-feldspar	1.64 ± 0.15	Insufficient datable material	-	Insufficient datable material			
GL20013	EC-022-VC	Quartz	1.00 ± 0.09	299.0 ± 34.1	299.2 ± 42.9 (40.8)	None	385.0-213.4	*N/A*	SP-3
		K-feldspar	1.83 ± 0.15	Insufficient datable material					
GL20014	EC-023-VC	Quartz	1.79 ± 0.17	618.6 ± 74.4	345.6 ± 52.7 (49.6)	D_e exceeds saturation threshold: accept as minimum age estimate	451.0-240.2	*321.1-219.9*	SP-2
		K-feldspar	2.42 ± 0.20	508 (Saturated)	>210	Saturated D_e value; accept as minimum age estimate			
GL20015	EC-023-VC	Quartz	1.65 ± 0.16	459.1 ± 40.5	277.8 ± 35.8 (32.9)	Significant feldspar contamination and D_e exceeds saturation threshold: accept as minimum age estimate	349.4-206.1	*330.0-236.5*	SP-2
		K-feldspar	2.30 ± 0.19	484 (Saturated)	>210	Saturated D_e value; accept as minimum age estimate			
GL20016	EC-023-VC	Quartz	2.73 ± 0.25	705.7 ± 83.9	258.7 ± 39.1 (37.0)	D_e exceeds saturation threshold: accept as minimum age estimate	336.9-180.5	*345.6-244.2*	SP-2
		K-feldspar	3.51 ± 0.28	424 (Saturated)	>117	Saturated D_e value; accept as minimum age estimate			

Table 5
Radiocarbon dates from VC091, Hornsea One ECC (Heamagi, 2018). Radiocarbon dates are calibrated against Marine20 (Heaton et al., 2020) with no ΔR correction applied. Core location shown in Fig. 3.

Lab code	Easting (WGS84 UTM31N)	Northing (WGS84 UTM31N)	Seabed elevation (m LAT)	Material dated and sample depth	Radiocarbon age (bp)	$\delta^{13}C_{VPDB}$ (‰)	Calibrated age (cal. BP)
SUERC-78242	352662	5941593	−39.7	Shell, 0.42m	41,876 ± 307	0.1	44,500–43,300
SUERC-78243	352662	5941593	−39.7	Shell, 1.08m	45,992 ± 485	−6.2	48,750–46,450

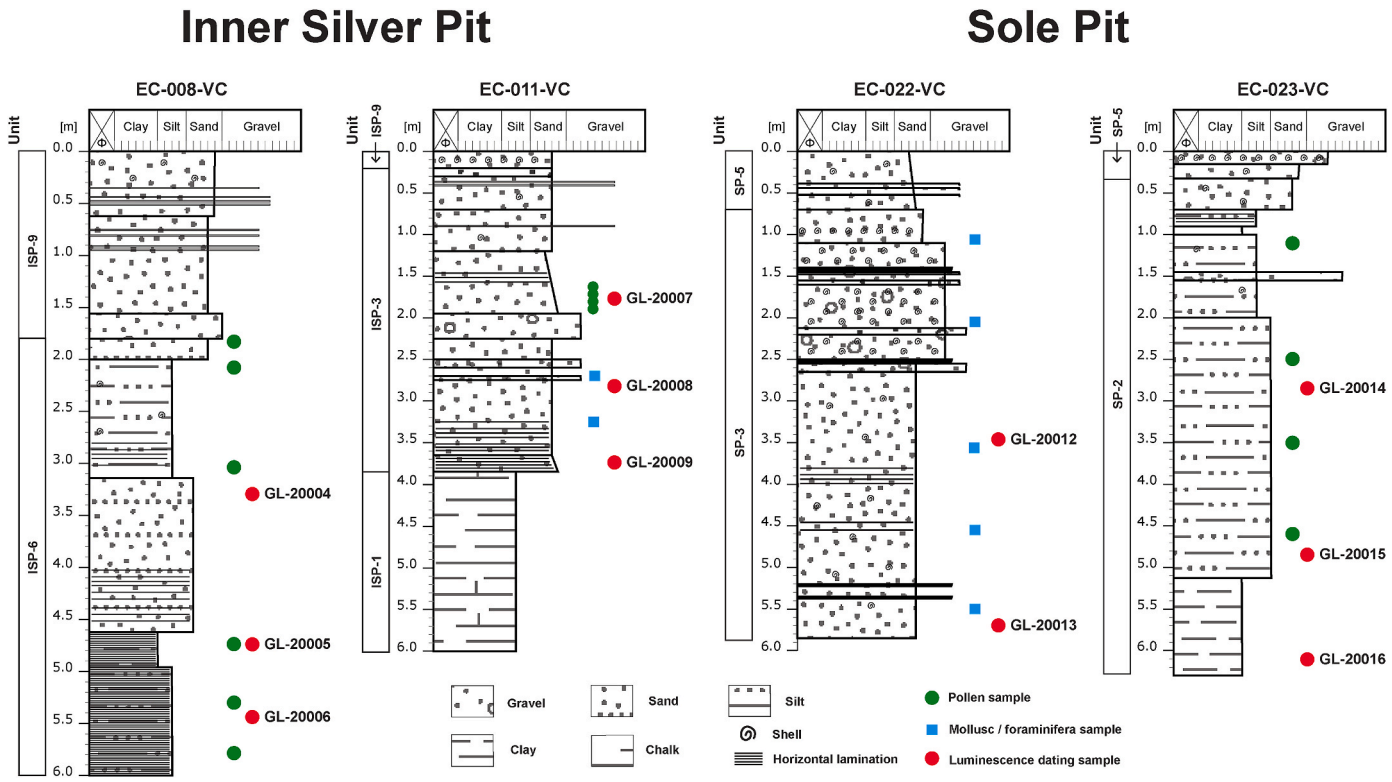


Fig. 4. Sedimentary log showing luminescence dating and biostratigraphic sampling for cores EC-008-VC, EC-011-VC, EC-022-VC and EC-023-VC. Core descriptions and photographs are provided in Supplementary Material S2.

Botney Cut Formation, producing ages close to the limit of radiocarbon dating, very likely to be 'ghostdates' pre-dating 55 ka (see Busschers, 2012; Busschers et al., 2014). These dates provide a TAQ for the age of the ISP-6 deposit. ISP-6 has a maximum vertical thickness of ~5.8 m (7.3 ms TWT).

An unconformity separates ISP-6 from the overlying unit, ISP-7, which forms an extensive tabular deposit with a very strong near-horizontal base reflector, characteristic of the Bolders Bank Formation. This unit is locally eroded by channels (unit ISP-8 – not shown in Fig. 3) associated with the overlying Botney Cut Formation away from the ISP margins. The stratigraphic sequence is topped by unit ISP-9, a near-continuous, acoustically transparent surficial unit with occasional small seismic anomalies (likely buried boulders), which yielded samples consisting of loose to very dense sand with gravel and shell fragments, and was assigned to the Southern Bight Formation.

Two vibrocores from the Inner Silver Pit were analysed, sampling the base of unit ISP-3 (EC-011-VC) and unit ISP-6 (EC-008-VC) (see Fig. 3 and Fig. 4).

4.1.1. Core EC-011-VC

EC-011-VC was taken from the ISP base. The bathymetry reveals a palaeochannel oriented east-west, cutting into the chalk as it crosses the terrace on the eastern side of the ISP. This channel disappears as it enters the deepest part of the ISP. The channel can be traced into the eastern face of the ISP, aligning with the base of unit ISP-3 (LSHF).

Lithology: the core consists of an eroded chalk surface (ISP-1) at 3.84 m, overlain by 3.15 m of a greyish gravelly silty sand channel fill (ISP-3), topped by 0.69 m of modern marine sands (ISP-9) (Fig. 4).

The ISP-3 channel deposits consist of a basal sand that grades into the overlying silt loam, with laminated black sand present between 3.66 and 3.64 m. Above this, the sediment coarsens, with a shift from fine to medium to coarse, poorly graded sand between 3.64 and 2.25 m, topped by a gravelly loam between 2.25 and 1.95 m. This is capped by coarse sand that, above 1.70 m, transitions into a well-graded sandy loam towards the top of the palaeochannel sequence, finally overlain by marine sands (ISP-9).

Chronology: the three quartz OSL dates contained significant feldspar contamination and were therefore accepted only as minimum ages, with the basal quartz OSL date (GL20009Q) providing an age of 301.9-145.5 ka b2k (95% probability). pIRIR dating of the K-feldspar, however, yielded dates with no associated caveats for GL20007F and GL20009F. GL20008F failed due to insufficient datable material. These dates are significantly older than the minimum age estimates derived from the quartz OSL, with GL20009F providing an age of 530.0-349.2 ka b2k (95% probability). Following construction of a Sequence model (Fig. 5), which showed good overall agreement (Amodel = 108), the basal date (GL20009F) provided a posterior density estimate of *520.2-378.3 ka b2k* (*GL20009F; 95% probability*), most likely *480.0-409.9 ka* (*68% probability*). This date is most likely associated with MIS 12 (*55.2% probability*), with a *26.1% probability* of being associated with MIS 11. The date from the top of the sequence (GL20007F) provided a posterior density estimate of *474.8-343.0 ka b2k* (*GL20007F; 95% probability*), most likely *443.9-377.8 ka b2k* (*68% probability*). This date is most likely associated with MIS 11 (*53.8% probability*), which spans 424-374 ka (Lisiecki and Raymo, 2005), with a *30.0% probability* of being associated with MIS 12. The pIRIR dating therefore places the channel fill as Late MIS 12 (Anglian glaciation) to early MIS 11 (Hoxnian interglacial), consistent with its stratigraphic position at the interface between units ISP-2 (Swarte Bank Formation) and ISP-3 (LSHF).

Pollen: pollen was preserved between 1.88 and 1.64 m, dominated by *Pinus* (40-50% TLP) with Poaceae and Cyperaceae (10-15% TLP each) (Fig. 6). Woodland components contribute up to 70% TLP, with *Picea*, *Betula* and *Alnus glutinosa* the most prevalent woodland taxa after *Pinus*. Local *Picea* is confirmed by a stomata cell (identified following Finsinger and Tinner, 2020) present at the base of the sequence. This assemblage suggests a late glacial/early interglacial assemblage, as implied by the presence of *Saxifraga granulata*-type, *Helianthemum*, *Cryptogramma* and *Isoetes lacustris*. Chenopodiaceae and *Plantago maritima* indicate local

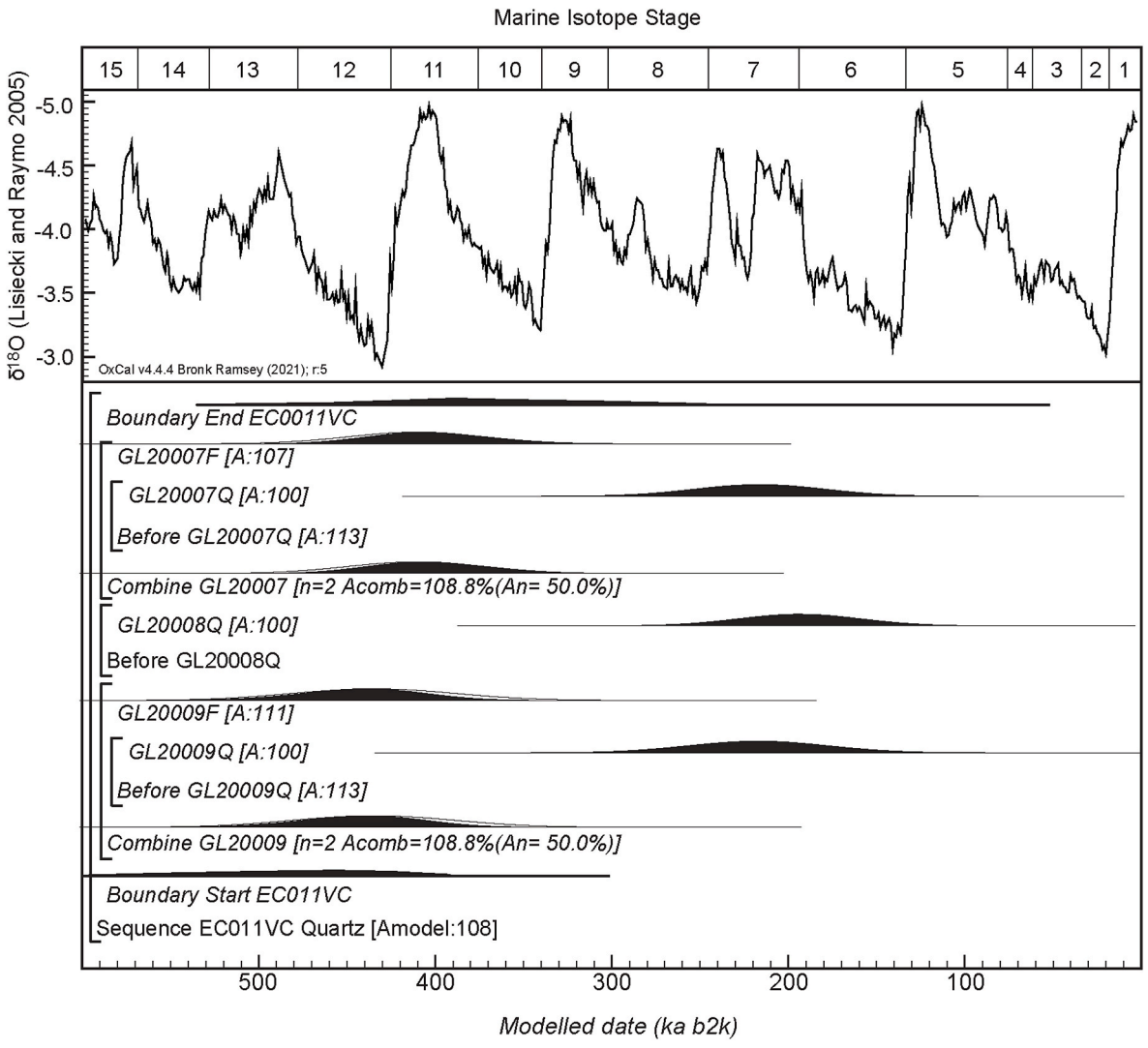


Fig. 5. Bayesian chronological model for luminescence dates from EC-011-VC in unit ISP-3 (Lower Sand Hole Formation; see Tables 3 and 4). The large square brackets down the left-hand side of the diagram, together with the OxCal keywords, define the overall model exactly.

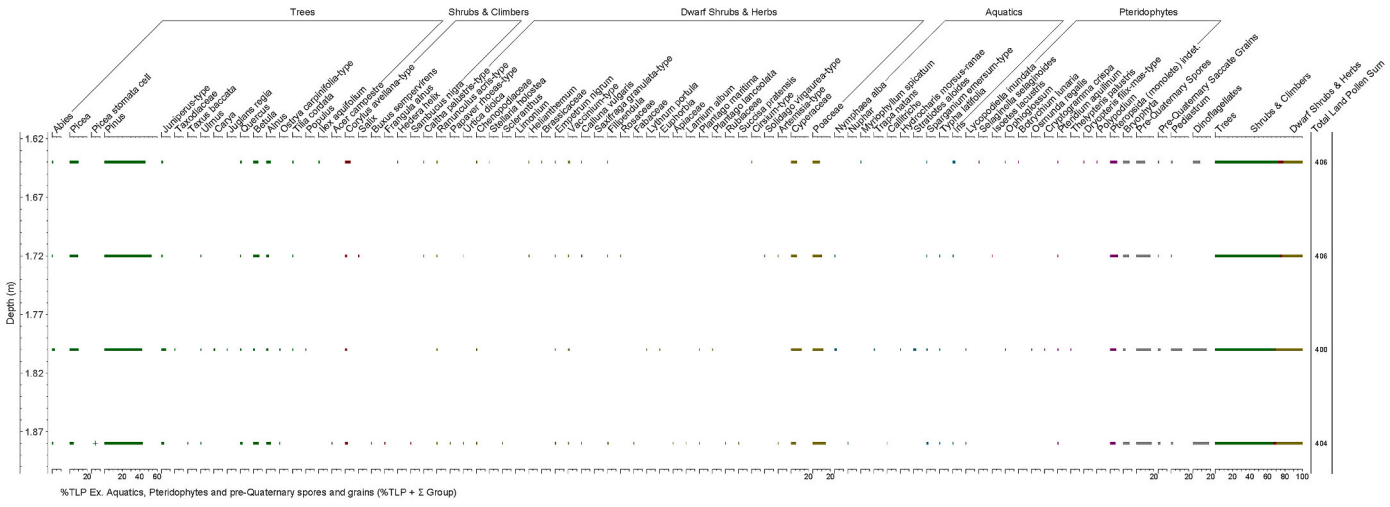


Fig. 6. Pollen diagram for samples from EC-011-VC (unit ISP-3; Lower Sand Hole Formation). Sample locations are shown in Fig. 4.

Table 6
Estimated abundance of foraminifera in EC-011-VC (unit ISP-3; Lower Sand Hole Formation). Sample locations are shown in Fig. 4.

Depth (m)		2.65 - 2.73	3.20 – 3.30
Weight before processing (g)		290	280
FORAMINIFERA	Group		
Ammonia cf. *aberdoveyensis* (Haynes, 1973)	(F)1 – intertidal and saltmarsh benthic	+	1
Bulimina marginata (d'Orbigny, 1826)	(F)2 – inner shelf, benthic	+	
Melonis affinis (Reuss, 1851)	(F)2	+	
Globigerina bulloides (d'Orbigny, 1826)	(F3) - planktonic	+	

Scale of estimated abundance: + = 1-10 items.

proximity to brackish environments, along with a constant presence of dinoflagellate cysts. *Empetrum nigrum*, *Calluna vulgaris*, *Vaccinium*-type and *Scleranthus* indicate the presence of heath. *Buxus sempervirens* is present at the base of the sequence and was also observed by Scourse et al. (1998) in their samples from the Sand Hole Formation. Damp ground is suggested by the presence of *Caltha palustris*-type, *Filipendula*, *Lythrum portula* and *Thelypteris palustris*, with *Frangula alnus* indicating damp woodland and *Iris* indicating wet ground or open water. *Nymphaea alba*, *Hydrocharis morsus-ranae*, *Sparganium emersum*-type, *Typha latifolia* and *Stratoides aloides* indicate the presence of slow-moving or still water. *Carya*, *Ostrya carpinifolia*-type, and Taxodiaceae were also present, along with high concentrations of pre-Quaternary spores and saccate pollen, the latter exhibiting differential staining, which Stanley (1966) observed can reflect exine-chemistry changes that occur during the reworking process. These suggest a significant reworked-material component, likely also contributing to the elevated arboreal (notably *Pinus*) component, especially if deposited in an estuarine environment (Traverse and Ginsberg, 1966; Liénart et al., 2022).

Foraminifera: low numbers of foraminifera were present below 2.65 m, broadly indicating an inner shelf environment (Group F(2)) (Table 6). The genus *Ammonia* requires taxonomic clarification globally (Hayward et al., 2004). However, the form represented here most closely resembled *Ammonia aberdoveyensis*, which tends to occur in brackish waters such as estuaries and lagoons, whereas *Ammonia batava* tends to occur in open-sea, inner-shelf settings. The tests present all lacked the umbilical boss of *Ammonia batava*, but the possibility that they are an intermediate form remains.

Summary: unit ISP-3 was likely deposited within a brackish channel during late MIS 12/early MIS 11. This is consistent with ISP-3 being classified as LSHF.

4.1.2. EC-008-VC

Vibrocore EC-008-VC was collected from the western margin of the ISP to sample unit ISP-6 (see Fig. 3).

Lithology: the core contains laminated silty clay loam that transitions to laminated sandy clay above 4.96 m, with horizontally laminated silty clay loam interbedded with silty sand layers above 4.61 m, and is topped by marine sands (ISP-9) above 1.8 m (Fig. 4). The particle size distribution (PSD) shows broad consistency throughout the sequence and is comparable to the unit ISP-6 deposits from EC-013-VC, VC091, and VC093 (Fig. 7). These generally have a higher proportion of medium-to coarse-silt and a lower sand component than the silty clays associated with the unit ISP-4 Sand Hole Formation encountered in EC-011-VC and VC085a. However, a sand layer at 4.25 m in EC-008-VC is a well-graded fine sand and shows a stronger correlation with the deposits in EC-011-VC, which are distinct from the marine sands in units ISP-5 and SP-2 (Egmond Ground Formation).

Chronology: all three pairs of OSL and pIRIR dates (GL20004-6) passed the Ward and Wilson (1978) test, indicating consistency between the two methods. The Sequence model showed good overall agreement (Amodel = 101; Fig. 8) and was consistent with the TAQ provided by the two radiocarbon dates from VC091. The basal date (GL20006) yielded a posterior density estimate of *84.3-70.2 ka b2k* (*Combine GL20006; 95% probability*). This date is statistically most likely to be associated with MIS 5a (*88% probability*). Dates GL20004 and GL20005 are also statistically most likely to be associated with MIS 5a (*79% and 62% probabilities*, respectively). This makes the EC-008-VC sequence younger than

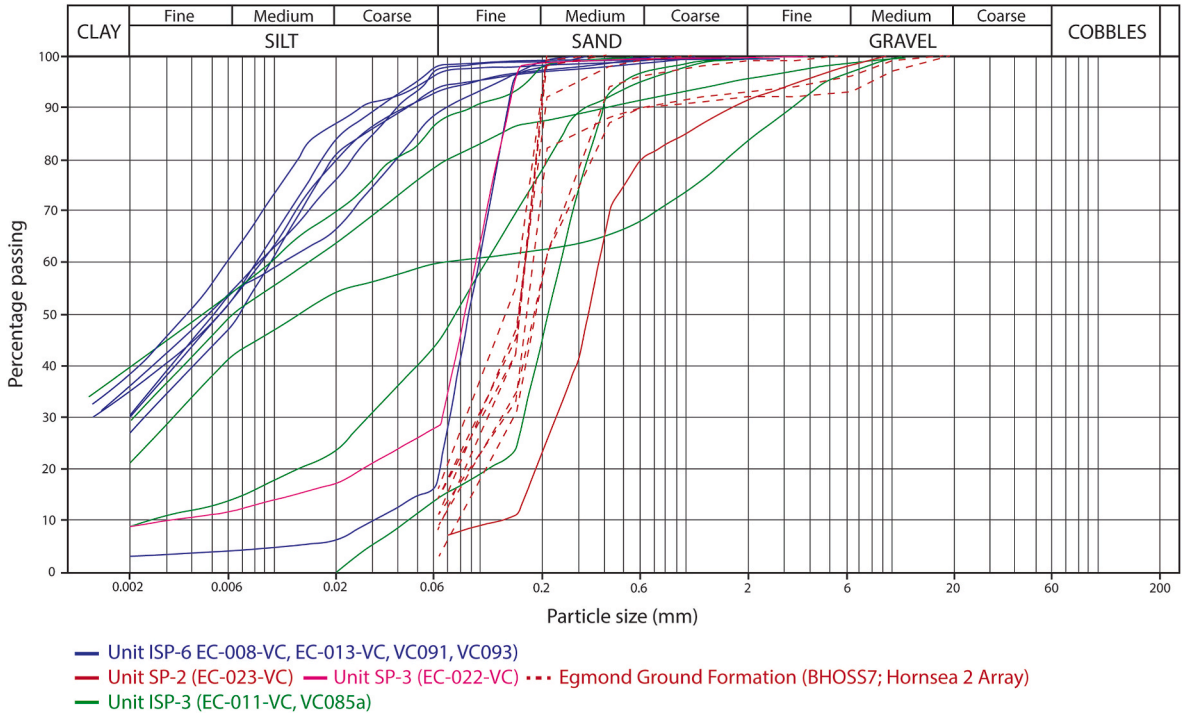


Fig. 7. Comparison of particle size analysis results, categorised by associated Pleistocene Formation. Data from the Egmond Ground Formation within BHOSS7 PSA in the Hornsea Two Array area (see Fig. 1 for location) are also included for comparison.

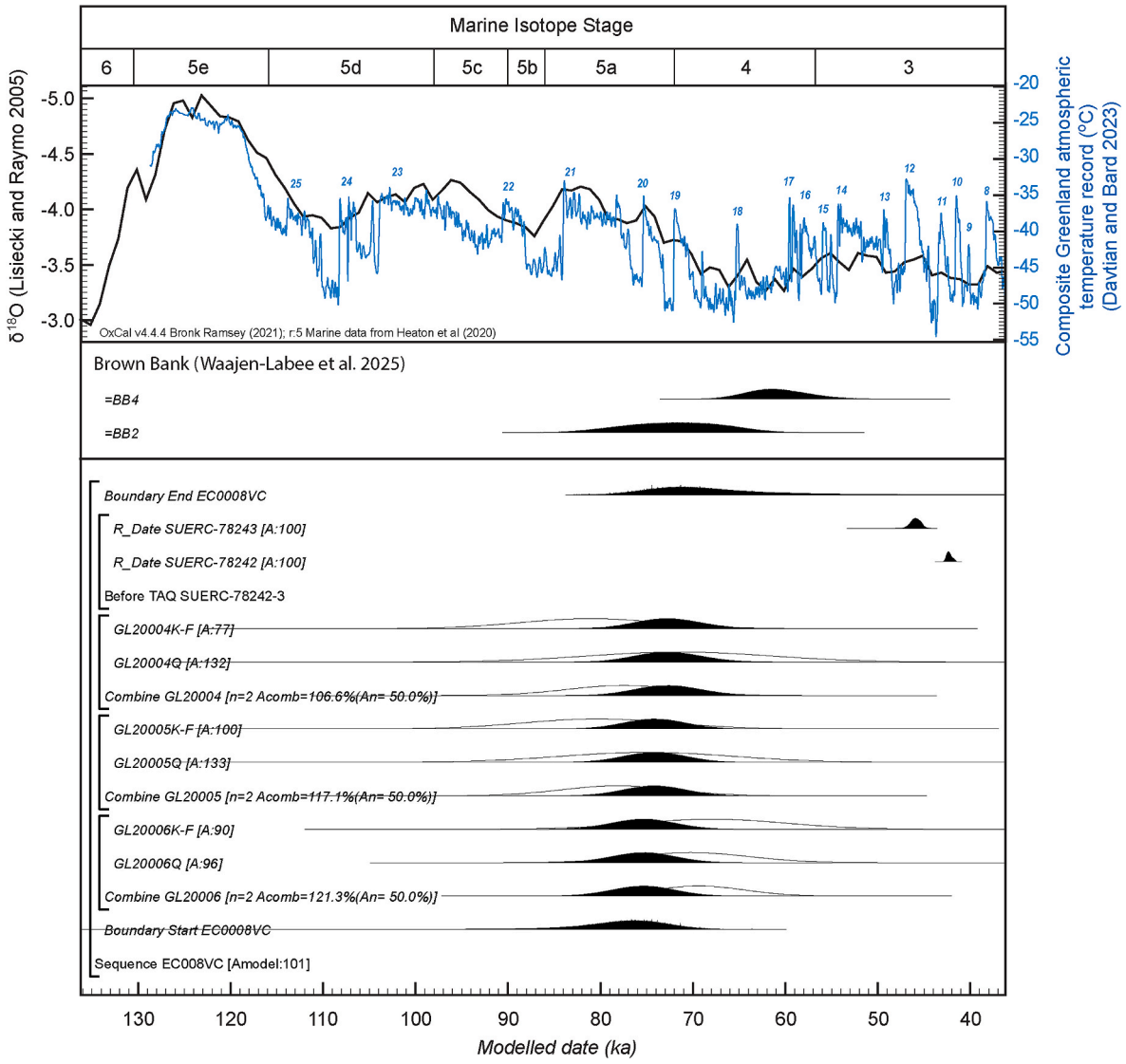


Fig. 8. Bayesian chronological model for luminescence dates from EC-008-VC in unit ISP-6 (Brown Bank Formation; see Tables 3 and 4), incorporating SUERC-78242 and SUERC-78243 from VC091 as a TAQ (see Table 5). The large square brackets down the left-hand side of the diagram, together with the OxCal keywords, define the overall model exactly. For comparison, modelled ages for BB2 and BB4 from the Brown Bank Formation (Waajen-Labee et al., 2025) are shown. Dates for MIS 5 sub-stages are based on those provided by Thompson and Creveling (2021). Blue numbers represent Greenland Interstadials (Rasmussen et al., 2014), plotted against the composite Greenland atmospheric temperature record (Davtian and Bard, 2023).

the British Chelford Interstadial, dated c. 100-90 ka (MIS 5c; Rendall et al., 1991), and instead correlates with the British Brimpton Interstadial, dated c. 80 ka (MIS 5a; Stone et al., 2012). The age of this deposit matches that of the Brown Bank Formation provided by Waajen-Labee et al. (2025) (Fig. 8).

Pollen: pollen was present throughout the core, though preservation and concentrations were moderate, only permitting limited counting to ~250 TLP (Fig. 9). The assemblage is dominated by *Pinus*, Cyperaceae and Poaceae. Woodland components contribute up to 30% TLP, including *Abies*, *Betula*, *Alnus glutinosa* and *Corylus avellana*-type in most samples, along with some *Picea* and *Quercus*. The presence of Chenopodiaceae, *Limonium*, *Armeria maritima*, *Plantago maritima,* and *Ophioglossum* indicates proximity to brackish and coastal environments. *Malva sylvestris*-type, *Linum catharticum* and *Botrychium lunaria* probably indicate local grassland or moorland, possibly on sandy soils, and are likely to be associated with *Empetrum nigrum*, *Scleranthus* and *Selaginella selaginoides*. Peaty soils are also indicated by *Calluna vulgaris*, *Drosera rotundifolia*-type and *Lycopodium inundata*. *Nuphar*, *Hydrocharis morsus-ranae*, *Sparganium emersum*-type and *Stratoides aloides* indicate slow-moving or still water, with the latter also commonly associated with calcareous conditions. The assemblage suggests late interglacial/interstadial. The increased abundance of *Pediastrum* (a genus of green algae) at the base of the sequence suggests some freshwater input, though fragmentation of many coenobia could suggest that these are derived from older reworked deposits. Reworked sediment is also suggested by the presence of *Carya*, *Pterocarya fraxinifolia* and *Ostrya carpinifolia*-type, coupled with high concentrations of pre-Quaternary spores and saccate pollen. Many of the pollen grains showed some signs of corrosion and degradation, which might further indicate some reworking of this assemblage.

This assemblage is very similar to the unit ISP-6 assemblage from VC093, which is also dominated by *Pinus*, with *Picea* and *Abies* present, and shows a high abundance of pre-Quaternary spores. By contrast, the assemblage in VC091 (Langdon and Scaife, 2018), also assigned to unit ISP-6, was dominated by Poaceae and Pteropsida (monolete) indet., with *Betula*, probably *Betula nana*, *Salix*, Cyperaceae, *Typha angustifolia*-type and *Pediastrum* also abundant, probably indicating a more open grass-sedge-tundra assemblage with steppe elements, with diatoms

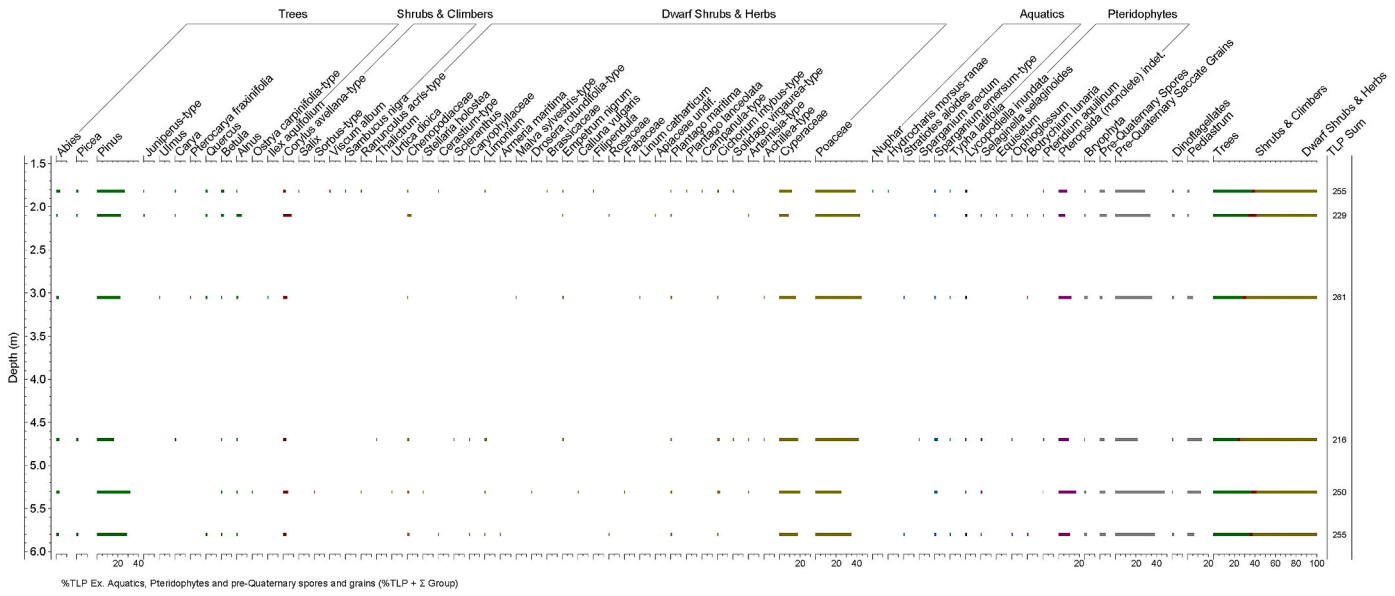


Fig. 9. Pollen diagram for samples from EC-008-VC (unit ISP-6; Brown Bank Formation). Sample locations are shown in Fig. 4.

showing that deposition was within a brackish-marine environment (Cameron, 2018).

Summary: the unit ISP-6 laminated silty clay loam suggests the presence of shallow marine/estuarine deposits dated to MIS 5a/4.

4.2. Sole Pit crossing

The sedimentary sequence at the northern end of the SP is simpler than that observed within the ISP (see Table 1) and is divided into five stratigraphic units. An example seismic profile across the northern end of the SP is shown in Fig. 10.

Jurassic bedrock (SP-1) underlies the entire area and is characterised by a strong upper boundary reflector and dipping reflectors throughout. Bedrock exposure is also visible at the base of the SP, indicating a north-south strike orientation. Bedrock exposure diminishes to the south of the coring locations, where thick fills (SP-5) of probable Southern Bight, though possibly Botney Cut, Formation, are present, up to 16 m (20 ms TWT) thick. Within the margins of SP, a clearly defined, acoustically transparent to weakly horizontally bedded seismic unit (SP-2) lies directly above the bedrock, up to 24 m (30 ms TWT) thick, and is correlated with the Egmond Ground Formation. On the eastern side of SP, an irregularly shaped and structured mass (unit SP-3), likely attributable to mass movement on the valley margin, is present. A strong reflector separates SP-2 and SP-4, located up to 18.4 m (23 ms TWT) below the seabed, marking the base of the Bolders Bank Formation. This is overlain by a near-continuous, surficial, acoustically semi-transparent unit (SP-5) with near-surface dipping reflectors associated with bedforms visible in the bathymetry, attributed to the Southern Bight Formation.

Two vibrocores from the Sole Pit, SP-2 (EC-023-VC) and SP-3 (EC-022-VC), were subjected to analysis and sampling.

4.2.1. EC-023-VC

EC-023-VC, taken from the eastern margin of SP, is positioned on the slope just west and below the stratigraphic boundary between units SP-2 (Egmond Ground Formation) and SP-4 (Bolders Bank Formation; Fig. 10).

Lithology: the core consists of 0.32 m of greyish-brown sandy clay overlain by 6.00 m of sandy loam (SP-2), dominated by the fine-sand fraction, topped by marine sands (SP-5) (Fig. 4). The PSD shows grading comparable to that of other units associated with shallow-marine to intertidal deposits (Fig. 7). The colour and lithology of the sediments match those reported for the Egmond Ground Formation (e.g. Ansari, 1992; Arlott et al., 2023).

Chronology: D_e values for all three quartz OSL samples exceeded the saturation threshold, and significant feldspar contamination was also evident in GL20015Q, so these dates should be accepted only as minimum ages. pIRIR dating of the K-feldspar component also yielded saturated D_e values for all samples, with these dates providing TAQs between 117 and 210 ka. A Sequence Model was used to assess the chronostratigraphic consistency of these age estimates, identify potential outliers (see Bronk Ramsey, 2008), and provide TAQ estimates for the SP-2 deposit.

The Sequence model (Fig. 11) had good overall agreement (Amodel = 86), although GL20014Q had poor agreement with the model (A = 58.0% (A'c = 60.0%)), falling just below the agreement threshold. The basal date (GL20016Q) provided a posterior density estimate of *345.6-244.2 ka b2k* (*GL20016Q*; *95% probability*), and most likely *318.8-268.3 ka b2k* (*68% probability*). This date is statistically most likely to be associated with MIS 8 (*60% probability*), with a *33.5% probability* of being associated with MIS 9 (Purfleet Interglacial). Dates GL20015Q and GL20014Q are also statistically most likely to be associated with MIS 8 (*73.4%* and *72.7% probabilities*, respectively). Although these dates should be considered TAQs, due to the saturated D_e values, they are comparable to date GL20013Q from EC-022-VC, also attributed to the Egmond Ground Formation.

Pollen: the pollen assemblage (Fig. 12) is dominated by *Pinus* (up to 65% TLP), with Poaceae and Cyperaceae (up to 25% TLP each) and *Picea* (up to 8% TLP). *Betula*, *Alnus glutinosa* and *Corylus avellana*-type are present throughout at low percentages (<5% TLP). *Empetrum nigrum* and *Vaccinium*-type are present throughout the sequence, along with occurrences of *Calluna vulgaris,* suggesting heath communities, likely associated with *Selaginella selaginoides* and *Lycopodium inundata*. Chenopodiaceae, *Armeria maritima* and *Plantago maritima* indicate local proximity to brackish environments. Local wetland is indicated by the presence of *Caltha palustris*-type, *Thalictrum*, *Filipendula* and *Glyceria*-type. Local standing or slow-moving water is signalled by the presence of *Nymphaea alba* and *Sparganium emersum*-type, along with *Iris*. *Equisetum* is present, notably at 2.51 m, which may be associated with dune-slacks, river or lake edges, or other damp grassland sites. The presence of *Azolla filiculoides-type* microsporangium, with its characteristic anchor-shaped glochidia, may also indicate local standing or slow-moving water.

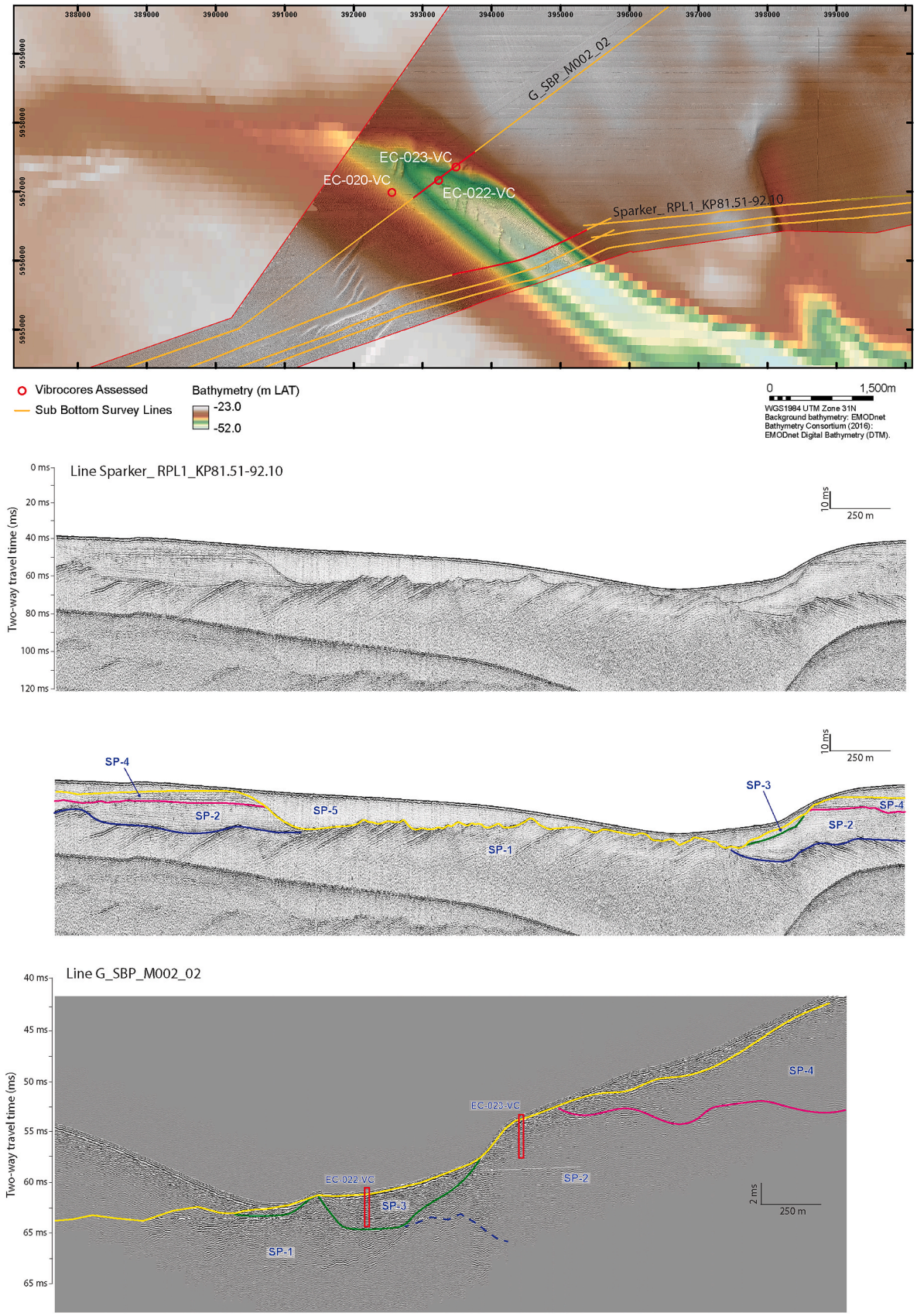


Fig. 10. Geophysical profile across the Sole Pit. Sparker line RPL1_KP81.51-92.10 shows the structure of the pit, clearly identifying the underlying geological surface and the presence of the Egmond Ground and Bolders Bank Formations at the eastern and western margins. Pinger line G_SBP_M002_02 has lower penetration but shows the seismic stratigraphy at the EC-022-VC and EC-023-VC coring locations and the relationship of the cores to the local Pleistocene Formations. See Table 1 for a summary of Quaternary Formations.

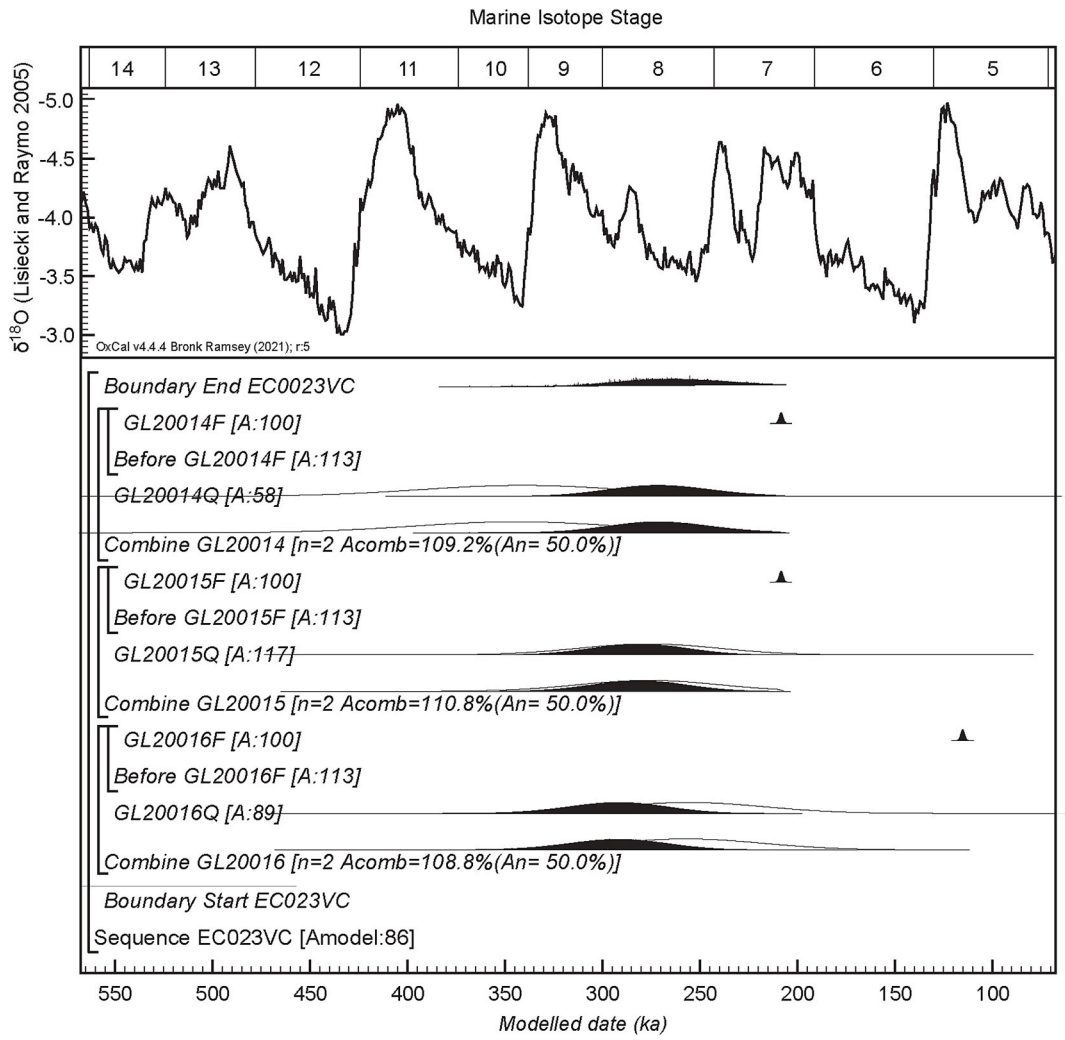


Fig. 11. Bayesian chronological model for luminescence dates from EC-023-VC in unit SP-2 (Egmond Ground Formation; see Tables 3 and 4). The large square brackets down the left-hand side of the diagram, together with the OxCal keywords, define the overall model exactly.

These are often found in Hoxnian interglacial or earlier deposits, though they have also been recorded during the MIS 9 Purfleet interglacial (Bridgland et al., 2001; Roe and Preece, 2011). Cameron et al. (1992: 111) note that the Egmond Ground typically contains spores of *Azolla filiculoides*, implying that it might be a useful biostratigraphic marker. Occasional grains of *Pterocarya fraxinifolia*, *Ostrya carpinifolia*-type, Taxoidiaceae and pre-Quaternary spores are present, but their low abundance suggests a limited reworked component, with pollen preservation generally good in all samples.

Summary: Unit SP-2 was likely deposited during late MIS 9/8 in a shallow marine environment, possibly near a shoreline. Unit SP-2 is correlated with the Egmond Ground Formation.

4.2.2. EC-022-VC

Vibrocore EC-022-VC was taken from the base of the SP in unit SP-3 (Fig. 10).

Lithology: at the base of the core, 1.5 m of poorly graded sand (58% medium sand; Fig. 5) overlain by shelly sandy gravels and sand (SP-3) is topped by a shelly sand above 0.70 m associated with SP-5 (Fig. 4). The PSD matches that of the Egmond Ground Formation sampled at the WTG site (e.g. BHOSS7: Fig. 7), with increased grading compared with that seen in EC-023-VC. The core was taken from a feature interpreted as an irregularly shaped, structured mass, likely emplaced during the Devensian, when overriding grounded ice led to mass movement of the SP-2 Egmond Ground Formation along the tunnel valley margins (Kirkham et al., 2021; Prins et al., 2020).

Chronology: the quartz OSL fraction provided ages of 687.7-348.9 ka b2k (GL20012Q; 95% probability), most likely 605.5-431.0 ka b2k (68% probability), while the underlying date GL20013Q provided an age of 385.0-213.4 ka b2k (95% probability), most likely 343.4-255.0 ka b2k (68% probability). pIRIR dating of the K-feldspar component within samples GL20012F and GL20013F was unsuccessful due to insufficient datable material. For GL20012Q, the sample consideration is that D_e exceeded the saturation threshold and should therefore be accepted only as a minimum-age estimate, whereas the underlying date GL20013Q had no such sample considerations. Date GL20012Q correlates with MIS 16 to 12, whereas GL20013Q correlates with late MIS 10 to late MIS 8. The likelihood that these deposits slumped may account for the mixed dates from the core, with older reworked material incorporated into the upper part of the sequence. The similarity of date GL20013Q to those from EC-023-VC (GL20014-GL20016) in unit SP-2 increases confidence in a valley margin slumping hypothesis and that SP-3 is derived from the Egmond Ground Formation.

Foraminifera and molluscs: these are present throughout the core (Table 7). At 5.45-5.55 m, *Ammonia batava* and *Ammonia* cf. *aberdoveryensis*, along with *Melonis affinis*, indicate subtidal to inner shelf conditions. A series of M(1) and M(2) species are present, with the former more abundant, probably indicating proximity to the tidal frame. At

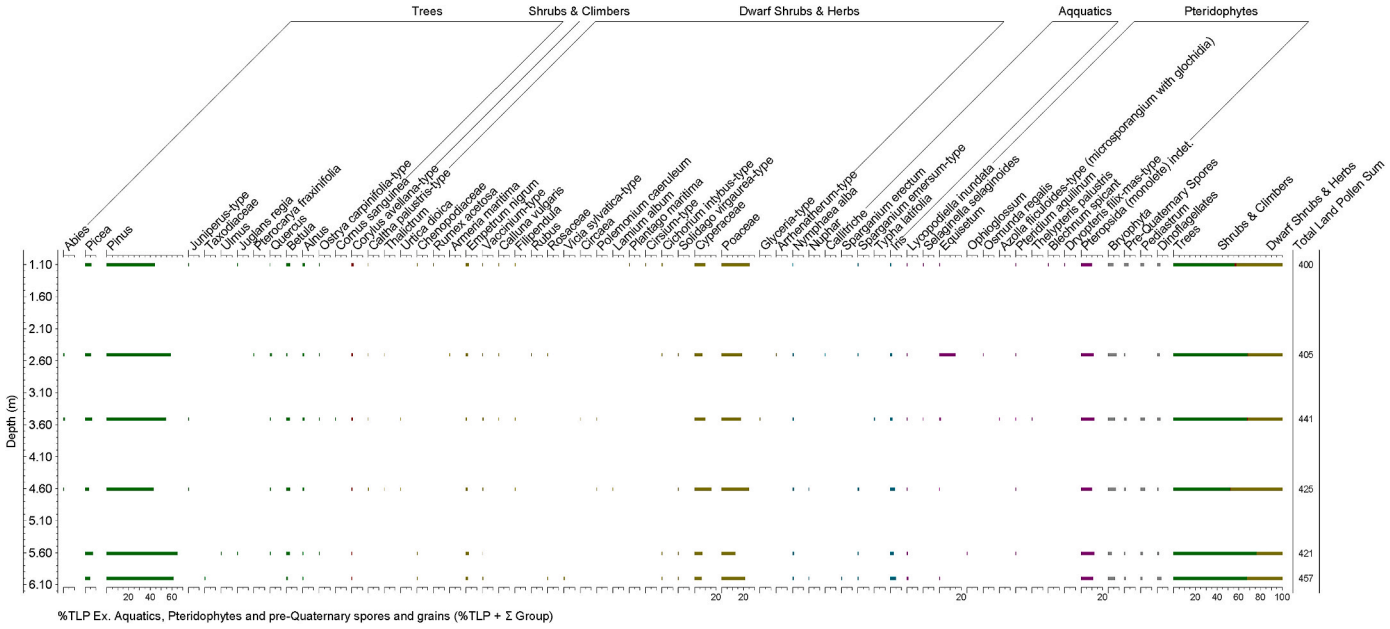


Fig. 12. Pollen diagram for samples from EC-023-VC (unit SP-2; Egmond Ground Formation). Sample locations are shown in Fig. 4.

4.50-4.60 m, *Ammonia* cf. *aberdoveyensis*, typically an intertidal species although it does occur sub-tidally, was present. The mollusc assemblage is dominated by *Tridonta montagui*, with *Astarte sulcata*, *Delectopecten vitreus* and a single *Rissoa membranacea*, an M(1) species associated with lower shores and subtidal settings. At 3.50-3.60 m, a single *Ammonia batava* test and a small assemblage of M(1) and especially M(2) molluscs, reflecting the sandy substrate, were present. At 2.00-2.10 m, molluscs and foraminifera are scarce. *Spisula solida* (Group M(1)) and *Astarte sulcata* (Group M(2)) suggest a sandy subtidal to inner shelf. Finally, at 1.00-1.10 m, an assemblage of Group F(2) foraminifera, dominated by *Ammonia batava* and *Quinqueloculina seminulum*, is present. The mollusc assemblage comprises M(1) and M(3) species, with the latter, especially *Timoclea ovata*, predominant. This assemblage suggests a subtidal to inner-shelf position with rocky substrates.

Summary: Unit SP-3 is interpreted as a slumped deposit at the valley margin, derived from unit SP-2. The deposits indicate a deepening of water depth, progressing from nearshore to deeper subtidal and inner shelf environments, most likely between late MIS 10 and late MIS 8. Unit SP-3 is correlated with the Egmond Ground Formation.

Table 7
Counts of foraminifera, molluscs and other invertebrates in EC-022-VC (unit SP-3; Egmond Ground Formation). Sample locations shown in Fig. 4.

Depth (m)		1.00 - 1.10	2.00 - 2.10	3.50 - 3.60	4.50 - 4.60	5.45 - 5.55	5.75 - 5.85
Weight before processing (g)		590	390	330	600	400	320
FORAMINIFERA	Group						
Ammonia cf. *aberdoveyensis* (Haynes, 1973)	(F)1				32	2	
Elphidium williamsoni (Haynes, 1973)	(F)1	1					
Ammonia batava (Hofker, 1951)	(F)1	18		1		13	
Ammonia sp. - broken	(F)1	1					
Quinqueloculina seminulum (Linnaeus, 1758)	(F)2	17					1
Melonis affinis (Reuss, 1851)	(F)2	1				10	
MOLLUSCA							
Anomia ephippium (Linnaeus, 1758)	M(1) – lower shore to subtidal, rocky to sandy substrates	1		1			
Steromphala cineraria (Linnaeus, 1758)	M(1)			1			
Buccinum undatum (Linnaeus, 1758)	M(1)	1					
Rissoa membranacea (J. Adams, 1800)	M(1)	1			1	5	
Spisula solida (Linnaeus, 1758)	M(1)	1	2			2	
Teretia teres (Reeve, 1844)	M(1)			1			
Tridonta montagui (Dillwyn, 1817)	M(2) – inner shelf, muddy to sandy substrates			9	24	5	
Astarte sulcata (da Costa, 1778)	M(2)		1	4	1	1	
Epitonium clathrus (Linnaeus, 1758)	M(2)			2			
Turritellinella tricarinata (Brocchi, 1814)	M(2)				1		
Aequipecten opercularis (Linnaeus, 1758)	M(3) – inner shelf, sandy to gravelly substrates	8					
Delectopecten vitreus (Gmelin, 1791)	M(3)					1	
Timoclea ovata (Pennant, 1777)	M(3)	17					
Cardiidae indet.							1
Unidentifiable fragment		1					1
CRUSTACEA							1
Barnacle plate				1			

5. Discussion

5.1. Sand Hole Formation

The oldest Pleistocene sequence sampled is in core EC-011-VC (unit ISP-3), which correlates with the onset of the Sand Hole Formation. The pollen record for the Sand Hole Formation was established by Ansari (1992), based on BGS Borehole 81/52, 11.5 km southwest of EC-011-VC on the western edge of Triton Knoll. This provided a record of the Hoxnian interglacial for the area, spanning the pre-temperate substage (Ho I), early-temperate (Ho II), late-temperate (Ho III), and post-temperate (Ho IV) stages. Fisher et al. (1969)) also generated pollen records from the ISP area using a series of gravity cores, though their relationship to the local Pleistocene stratigraphy was unknown; they simply stated that the cores were taken between the chalk and an overlying till. However, these pollen records appear to correlate with Hol IV.

The Hoxnian pollen record in borehole 81/52 correlates well with onshore Hoxnian records (see Forden, 2015), notably the lacustrine pollen records from Marks Tey, Essex (Turner, 1970; Tye et al., 2016). The Hoxnian pollen record has several distinct features, including a mixed deciduous woodland with *Picea* and abundant *Alnus* during Ho II; *Carpinus betulus* and *Abies* abundant during Ho III; and an abundance of *Pinus* and *Empetrum* during Ho IV. However, the Ho II record varies between sites, with Ansari (1992) reporting up to 40% TLP of *Picea* in the Sand Hole Formation, whereas in the Marks Tey sequence it never exceeds 10% TLP. The same pattern holds for the Ho I assemblage from Athelington, Suffolk (Coxon, 1985), where *Betula*, *Pinus* and Poaceae dominate.

The pollen record from EC-011-VC also differs from Ansari's (1992) findings for the Sand Hole Formation. This may, in part, be due to the latter having low pollen counts for Ho II and early Ho III, often fewer than 100 total pollen (TP), with pre-Quaternary taxa (PQT) comprising up to 50-70% TP + PQT. By contrast, in EC-011-VC, counts exceeded 400 TLP. Differences in preservation conditions between the two studies might account for the much higher abundance of boreal saccate grains in the borehole 81/52A Ho II and Ho III record than is observed at other onshore Hoxnian sites.

Reworked material is clearly present within the EC-011-VC assemblage, with variations in pollen preservation noted, consistent with Scourse et al. (1998), who reported that the lower section of borehole 51/52A consisted of a poorly preserved palynofacies with low concentrations dominated by residual reworked elements. Nonetheless, the pollen present is broadly consistent with its stratigraphic position, containing taxa expected in the pre-temperate phase (Ho I) of the Hoxnian interglacial and therefore predating the Sand Hole Formation pollen records of Ansari (1992), which were attributed to Ho II.

The abundance of dinoflagellate cysts in EC-011-VC may reflect a local marine influence, as evidenced by the presence of *Ammonia* cf. *aberdoveyensis*, albeit in limited abundance, which is associated with brackish water, such as in an estuary or lagoon. This is consistent with observations from the lower section of borehole 51/52A, where Kirkham et al. (2021) reports shallow marine dinoflagellate cysts and foraminifera.

Although the Sand Hole Formation is attributed to the Hoxnian, amino acid geochronology of its foraminifera by Kristensen et al. (1998) suggested correlation with MIS 9, whereas Scourse et al. (1998, 1999) state that these are still true Hoxnian (MIS 11) sequences. An MIS 11 age for Ho I is supported by the K-feldspar pIRIR from EC-011-VC, which indicates that the channel is late MIS 12 to early MIS 11, consistent with a late glacial/Ho I stage. This channel also constrains the age of the chalk terrace on the eastern side of the ISP, indicating that it had formed by the end of MIS 12, whereas the deeper channel area of the ISP to the west, where the channel is no longer visible and deeper incision of the chalk has occurred, must be post-MIS 12, probably eroded during a later glaciation when the ISP tunnel valley formed. While this terrace is a remnant of the late Anglian Stage, there is no evidence for a tunnel valley within which the Swarte Bank Formation sits in this area. Instead, it occupies a wide, shallow basin with localised channel incision into the underlying chalk.

Although no direct dates were obtained for the Upper Sand Hole Formation, the late MIS 12/early MIS 11 date from EC-011-VC supports an MIS 11 Hoxnian age for the LSHF, as proposed by Scourse et al. (1998). The luminescence dates from the stratigraphically younger Egmond Ground Formation provide a TAQ of late MIS 10 to MIS 8. Chronostratigraphically, the cross-bedded sands of the USHF are therefore most likely post-MIS 11, probably MIS 10 or 9. Arlott et al. (2023) proposed that their Unit B sand facies, at the top of the USHF, may represent part of the proto-Soar estuary. Gibbard et al. (2013; Belshaw et al., 2014) suggest that this might have formed after the Hoxnian interglacial, draining northward into the Wash and ISP, and that it persisted until the onset of glaciation during MIS 6. A possible MIS 10/9 age for the USHF is compatible with the proposed timing for a proto-Soar estuary in this area.

5.2. Egmond Ground formation

Cameron et al. (1992) propose a succession from the earlier Sand Hole Formation, deposited in a quiet, restricted marine environment during the interglacial, to the later Egmond Ground Formation, which formed as sea levels rose, creating more open-marine conditions. However, Arlott et al. (2023) have shown that this deposit is more complex, with distinct upper and lower fills, underlain by coastal or estuarine deposits consisting of channels and dune formations, which they reclassified as part of the USHF.

The Egmond Ground Formation is typically associated with Middle Pleistocene open-marine conditions, though its true age remains poorly understood. Stoker et al. (2011) and Dakin et al. (2026) attribute it to the MIS 11 Hoxnian interglacial. However, because the Sand Hole Formation contains a full MIS 11 record (Scourse et al., 1998), the overlying Egmond Ground Formation must be post-MIS 11. This is consistent with luminescence dating from EC-023-VC (TAQ of late MIS 9 through to MIS 8) and from GL20013Q from EC-022-VC (late MIS 10 through to late MIS 8). Paired luminescence dating of the Egmond Ground Formation has also been attempted within the Triton Knoll Offshore Wind Farm (BH-A03a; Toms and Wood, 2019a). The quartz OSL date (GL18025 Quartz) showed significant feldspar contamination, yielding a TAQ of 152.2 ± 20.0 ka (MIS 6), whereas the K-feldspar pIRIR date (GL18025 K-feldspar) failed the dose recovery test, yielding a terminus post quem (TPQ) of 361.8 ± 35.6 ka (MIS 10/9), which is statistically comparable to the date GL20014Q from the base of the EC-023-VC sequence.

Graham et al. (2011) correlate the Egmond Ground Formation of the southern North Sea with the upper section of the Ling Bank Formation of the central North Sea, noting floras similar to those from EC-023-VC. The age of the Ling Bank Formation is constrained by the overlying Fisher Formation, which Merritt et al. (2003: 62) suggest is no older than MIS 7 (Jensen and Knudsen, 1988; Holmes, 1997), while Stoker et al. (2011) provide a wider date range of MIS 10 to 6. Thermoluminescence dates from the base and centre of the Fisher Formation in borehole 81/29, Devil's Hole, yielded ages of 210 ± 20 ka and 182 ± 18 ka (Jensen and Knudsen, 1988), placing these within MIS 7/6. While the broad interpretation of the Fisher Formation is glaciomarine (Gatliff et al., 1994: 89; Merritt et al., 2003: 62), samples from Borehole 81/26 in the Fladen area demonstrate that the Fisher Formation is characterised by sediments deposited in a subglacial environment, including diamicton, during MIS 6 (Sejrup et al., 1987; Ekman and Scourse, 1993). If a correlation between the Egmond Ground and Ling Bank Formations is correct, then the MIS 6 glaciation should provide a TAQ for the Egmond Ground Formation.

It is therefore likely that deposition of the Egmond Ground Formation is younger than the ages adopted by Cameron et al. (1992), Stoker et al. (2011) and Dakin et al. (2026). This younger age aligns with the

model of Rijsdijk et al. (2005: Fig. 6b) for the Dutch sector of the North Sea, which suggests that the Egmond Ground Formation may span MIS 11 to 7. The presence of shallow marine to intertidal environments identified from this period is also compatible with the palaeogeography of the southern North Sea for the Late Middle Pleistocene presented by Hijma et al. (2012) and Cohen et al. (2017), which show active floodplains and deltas immediately south and west of the study area, while shallow sea and coast are centred on this area. At Triton Knoll, Arlott et al. (2023)interpreted the Egmond Ground Formation as being deposited within a coastal plain setting, consistent with Smith's (2019: 23) interpretation for the HOW02 WTG area, where thicker areas of the Egmond Ground Formation commonly feature low-amplitude chaotic to well-stratified reflectors, with sloping depositional foresets clearly visible, likely indicating intertidal deposition.

5.3. Brown Bank Formation

Resting unconformably above USHF (unit ISP-4), possibly with an intervening Egmond Ground Formation (ISP-5) on the western edge of the ISP, and immediately beneath the Bolders Bank Formation (ISP-7), is the laminated clayey loam deposit that we attribute to the Brown Bank Formation (ISP-6).

The paired luminescence dating, which produced coeval age estimates from quartz OSL and K-feldspar pIRIR, firmly places deposition in MIS 5a. This would be correlated with the British Brimpton Interstadial (Bryant et al., 1983). Similar to the pollen record from EC-008-VC, the Brimpton record shows dominance of open-ground taxa, notably high Poaceae, with *Pinus* most prevalent among the tree types; however, Brimpton shows a high abundance of *Betula*, which is not observed in the EC-008-VC or VC093 sequences but might be seen in the pollen from VC091 (Langdon and Scaife, 2018). Comparison can also be made with the pollen record from Cassington, Oxfordshire (Maddy et al., 1998). This has similar abundances of Poaceae, Cyperaceae, and *Pinus* to those seen in EC-008-VC, but notably a lower abundance of *Betula* than in the Brimpton record. Maddy et al. (1998) argued for a separate Cassington Interstadial after the Brimpton Interstadial, centred on the MIS 5/4 boundary, which is also compatible with the dating of the EC-008-VC record. Whether the Cassington and Brimpton Interstadials represent the same or separate interstadial phases, the pollen record from EC-008-VC and VC091, coupled with the dating, indicates a strong correlation with one or both of these. Rex et al. (2023) suggest that the Brimpton and Cassington Interstadials could be equivalent to the succeeding Odderade/St Germain II and Oerel/Ognon I Interstadials (Wohlfarth, 2013) at the MIS 5/4 transition around Greenland Interstadial (GI-) 21 to GI-19, consistent with the EC-011-VC dates (Fig. 8).

During site investigations for the Inner Dowsing OWF, 50 km southwest of EC-008-VC and ~3.5 km west of the main Wash channel connecting to the ISP to the north, Russell (2009) reported laminated sandy silty clay beneath the Bolders Bank Formation in borehole BHID25. This was interpreted as a freshwater glaciolacustrine deposit, with a pollen assemblage indicating deposition during a cold stage and showing similarities to that from EC-008-VC. The age of the sequence was determined by Amino Acid Racemisation, indicating deposition after MIS 7/6, probably no later than MIS 5c or 5a, which Russell (2009: 8)speculated might be equivalent to the Brown Bank Formation.

Within the eastern UK and Dutch sectors of the North Sea, the Eem Formation overlies the glacial deposits of the Drente Formation, attributed to MIS 6 (Rijsdijk et al., 2005), and is overlain by the Brown Bank Formation (extent shown in Fig. 1). Investigations at the Norfolk Boreas and Vanguard Offshore Wind Farms (Mellett, 2019a, 2019b; Eaton et al., 2020) attempted to OSL-date the Brown Bank Formation. At Norfolk Vanguard, dating yielded a wide range of dates spanning MIS 5b to 3 (Toms and Wood, 2019b), often with caveats attached to each date, while at Norfolk Boreas, two dates from VC016 (see Toms and Wood, 2019c), when subject to Bayesian chronology modelling, had a *66% probability* that the basal date (GL17153) and a *47% probability* that the upper date (GL17154) are MIS 5a, with the upper date also having a *46% probability* that it could be MIS 4.

Extensive luminescence dating of the Brown Bank Formation within the Dutch sector has been published by (Waajen et al., 2024; Waajen-Labee et al., 2025), using quartz OSL and K-feldspar pIRIR dating on multiple cores. This confirms that deposition of the Upper Brown Bank Formation occurred during MIS 5a to MIS 4 (Fig. 8).

Eaton et al. (2020) have characterised the Upper Brown Bank sediments as dark grey silts, sandy silts, and clays associated with a shallow-marine, intertidal, and/or lagoonal depositional environment. Notably, these are structureless deposits, unlike the laminated deposits present in EC-008-VC. However, Waajen-Labee et al. (2025) have identified laminated silty clays (lithofacies LF6) in seismic units BB2 and BB4, which they interpret as having been deposited in a relatively low-energy environment with relatively high sedimentation rates or dysoxic bottom conditions.

Chronological modelling of the dates reported by Waajen-Labee et al. (2025) yields posterior density estimates of *83.6-64.2 ka* (*95% probability*) for BB2, most likely *78.9-68.1 ka* (*68% probability*), and *68.9-55.7 ka* (*95% probability*) for BB4, most likely *66.2-59.6 ka* (*68% probability*). The dating of the EC-008-VC sequence is statistically indistinguishable from that of BB2 at the Brown Bank (Fig. 8).

(Waajen et al., 2024; Waajen-Labee et al., 2025) note that the onset of LF6 deposition contains significantly fewer *Pinus* and *Betula* than in lithofacies LF5 (strongly mottled silty clays), but shows an increase in other taxa, similar to that observed in EC-008-VC. Differences in taxon abundance may reflect spatial heterogeneity in vegetation structure, geology, local climate, or sample taphonomy.

Although preservation of diatoms, molluscs and foraminifera was poor in EC-008-VC, these were present in VC091 and VC093. Whittaker (2018) reports a few *Mytilus* juveniles and a rich microfossil assemblage of brackish ostracods and foraminifera (plus subsidiary freshwater ostracods) in VC091. The diatoms present were mainly non-planktonic marine, with marine-brackish species, suggesting deposition in shallow water (Cameron, 2018). Radiocarbon dating from VC091 confirms that this sequence is pre-MIS 2 (see Table 5), and seismic correlation shows that these deposits are the same as those encountered in EC-008-VC and EC-013-VC. Waajen-Labee et al. (2025) noted a reduced abundance of diatoms in LF6 compared to LF5 [which had an abundance of marine planktonic taxa]. Those present included abundant tychoplankton, epiphytes in low abundance, and planktonic taxa less abundant than in lithofacies LF5. LF6 contained an increase in marine-brackish taxa and fewer fully marine taxa than lithofacies LF5, which they interpreted as indicating shallower water conditions, with a decrease in salinity and potentially colder conditions compared to lithofacies LF5. The diatom assemblage from LF6 is therefore also comparable to that observed in the laminated clayey loam deposits from the ISP.

The strong similarity between the Brown Bank Formation deposits presented by Waajen-Labee et al. (2025) and those observed in the area around the ISP, both attributed to intertidal/shallow subtidal deposition and of equivalent age, provides greater confidence in classifying these deposits as Brown Bank Formation [equivalent].

Only a limited number of sea-level index points for MIS 5a globally (Creveling et al., 2017; Thompson and Creveling, 2021; Cohen et al., 2022). The ISP deposits, together with those from the Brown Bank Waajen-Labee et al. (2025) and those identified within Offshore Wind Farms in the eastern UK sector of the North Sea (see Dakin et al., 2026), therefore provide a significant resource for future studies of MIS 5a/4 sea-level change.

5.4. Opportunities for future offshore investigations

Paired luminescence dating has been successfully used to date Middle Pleistocene deposits in the southern North Sea. Most notably, it highlights the risk of relying solely on quartz OSL to date these

formations, especially when only minimum ages can be obtained. K-feldspar pIRIR offers significant opportunities to date deposits back to at least the MIS 12 Anglian glaciation. This is particularly useful when the quartz OSL signal is close to saturation, as seen in EC-023-VC for the Egmond Ground Formation. pIRIR is not guaranteed to produce accurate dates, and the slower bleaching time of the K-feldspar pIRIR signal means that careful consideration of sample taphonomy and the depositional environment is key to optimal sample selection. The paired dating approach allows some of these complexities to be explored, providing greater opportunities to produce robust site chronologies (as demonstrated by Waajen-Labee et al. (2025).

Biostratigraphy has been shown to support absolute dating, but the complex nature of these deposits means that some proxy techniques (such as pollen) cannot provide robust correlations with individual marine isotope stages, which are necessary for refining the region's chronostratigraphy (Rose, 2009; Thomas, 2001; Tzedakis et al., 2001). For example, Dakin et al. (2026: 31-32) discuss biostratigraphic evidence from the Egmond Ground Formation generated during Offshore Wind Developments, but this evidence lacks absolute dating and is therefore assumed to be MIS 11, as this is the age most commonly ascribed to the Egmond Ground Formation for the UK sector. Biostratigraphic techniques remain a critical component for evaluating these deposits, notably for understanding the complexities of the depositional environment and the potential position within a glacial-interglacial cycle (e.g. Iversen, 1958; West, 1970), but should not continue to serve as a substitute for absolute dating techniques (see Grant and Marshall, 2025a). Only through the adoption of more robust scientific dating programmes can the Middle Pleistocene stratigraphy of areas such as the southern North Sea be resolved. Such an approach should ultimately permit correlation between the Dutch and UK sectors, leading to a broader-scale understanding of the Quaternary subsurface geology. The identification of robustly dated deposits equivalent to the Brown Bank Formation, presented in this study and by Waajen et al. (2024), demonstrates that this is achievable.

The core handling procedures used by the geotechnical site investigation team have been shown to be suitable for the successful implementation of luminescence dating programmes, and this approach is already being adopted across the industry (e.g. Bynoe et al., 2022). The methodology presented provides a replicable workflow that should enable academic researchers to work with industrial partners to access core material without compromising geotechnical site investigation. However, success will still require early engagement between partners. This has the potential to increase opportunities to establish the age of Quaternary sedimentary sequences encountered during offshore marine infrastructure developments, thereby refining the interpretation of ground models generated from the extensive geophysical and geotechnical datasets collected.

This study has challenged existing assumptions about the age of these formations, demonstrating that the current chronostratigraphy for the Middle to Early Late Pleistocene still requires further investigation and robust scientific dating programmes to better understand their age and complexity. Achieving this will ultimately lead to a better understanding of the region's palaeogeography during this extended period. The identification of intertidal and coast-proximal deposits within these formations, traditionally attributed to marine environments, also highlights the potential for submerged palaeolandscapes suitable for Palaeolithic activity in this region, thereby requiring greater consideration and investigation through the current planning process (Westley and Bailey, 2013; Dix and Sturt, 2013; Peeters et al., 2009). This is particularly true of the Brown Bank intertidal/shallow-tidal deposits encountered around the ISP, as recent studies have shown that Late Middle Palaeolithic occupation in Britain may have occurred by MIS 5a rather than re-occupation in late MIS 4 (Shaw et al., 2024; Grant and Marshall, 2025b). The presence of probable contemporary late MIS 5 terrestrial (glaciolacustrine) deposits at the Inner Dowsing OWF confirms that remnants of this terrestrial and coastal palaeolandscape are preserved beneath the Bolders Bank Formation in the wider area. Future offshore developments that may encounter such deposits must therefore also be aware of the increased archaeological and geoarchaeological potential of these Middle to Early Late Pleistocene deposits.

6. Conclusions

The new protocol for core handling procedures, implemented during geotechnical site investigations for HOW02, has enabled the successful application of paired luminescence dating (quartz OSL and K-feldspar pIRIR) to Middle Pleistocene Formations in the area. The new dates confirm that the base of the Sand Hole Formation is late MIS 12 to MIS 11, with the Egmond Ground Formation likely to have accumulated through MIS 10 to 8; this is later than the currently adopted age of MIS 11 (Cameron et al., 1992; Stoker et al., 2011; Dakin et al., 2026) for the Egmond Ground Formation within the UK sector, aligning with the proposed chronology from the Dutch Sector for the Egmond Ground Formation of MIS 11 to 7 (Rijsdijk et al., 2005). A laminated intertidal/shallow tidal deposit, located above the Egmond Ground Formation on the margins of the Inner Silver Pit, has been shown to be chronologically, lithologically and biostratigraphically equivalent to the Brown Bank Formation, traditionally found only in the eastern southern North Sea and securely dated to late MIS 5a/early MIS 4. The new absolute dates provide much-needed clarity on the age of Middle to early Late Pleistocene Formations in this region and a partial revision of the existing chronostratigraphy for the southern North Sea.

Author contributions

Conceptualisation: M. Grant, S. Evans, P. Toms. Formal analysis: M. Grant, P. Toms, J. Wood, A. Smith, M. Law, T. Hill. Funding acquisition: S. Evans. Investigation: M. Grant, P. Toms, J. Wood, A. Smith, M. Law, T. Hill. Methodology: M. Grant, P. Toms, S. Evans, C. Walker. Project administration: S. Evans. Writing – original draft: M. Grant, P. Toms, S. Evans. Writing – review and editing: M. Grant, P. Toms, S. Evans, J. Wood, A. Smith, M. Law, J. Dix, C. Walker, T. Hill, C. Heamagi.

Declaration of competing interest

The authors declare that they have no known competing financial interests or personal relationships that could have appeared to influence the work reported in this paper.

Acknowledgements

The work was commissioned and funded by Ørsted as part of the Hornsea 2 development, with special thanks to Natalia Lopez and Jennifer Brack who facilitated the project, and Jennifer Ford, Tobias Naylor, Paul Kirk, Dirk Wilyman and Sara McLean. Staff at Ørsted and Fugro GB Marine Limited are thanked for their assistance and support throughout the project. Christopher Pater and Phillipa Naylor, Historic England Marine Planning Unit, are thanked for their advice throughout the process. Becky Briant and an anonymous reviewer are thanked for reviewing the original manuscript and providing valuable suggestions that helped improve this manuscript. Rachel Harding at MSDS Marine is also thanked for providing additional comments on this manuscript.

Appendix A. Supplementary data

Supplementary data to this article can be found online at https://doi.org/10.1016/j.quascirev.2026.110261.

Data availability

A link to the data and/or code is provided as part of this submission.

References

Adamiec, G., Aitken, M.J., 1998. Dose-rate conversion factors: new data. Ancient TL 16, 37–50. https://doi.org/10.26034/la.atl.1998.292.

Allcock, A.L., Hayward, P.J., Wigwam, G.D., Yonow, N., 2017. Molluscs (Phylum Mollusca). In: Hayward, P.J., Ryland, J.S. (Eds.), Handbook of the Marine Fauna of North-West Europe. Oxford University Press, Oxford, pp. 455–602.

Ansari, M.H., 1992. Stratigraphy and palaeobotany of Middle Pleistocene interglacial deposits in the North Sea. Unpublished PhD Thesis. University College of North Wales. https://research.bangor.ac.uk/en/studentTheses/stratigraphy-and-palaeobotany-of-middle-pleistocene-interglacial.

Arlott, L., James, L., Christopher, N., Duffy, C., 2023. The sand hole formation - winding back the clock to support ground modelling at Triton Knoll Offshore Wind Farm. In: Offshore Site Investigation Geotechnics 9th International Conference Proceeding, pp. 827–835. https://doi.org/10.3723/ZWLD9842.

Belshaw, R.K., Gibbard, P.L., Murton, J.B., Murton, D.K., 2014. Early Middle Pleistocene drainage in southern central England. Geol. Mijnbouw 93–4, 135–145. https://doi.org/10.1017/njg.2014.25.

Bennett, K.D., 1994. Annotated Catalogue of Pollen and Pteridophyte Spore Types of the British Isles. Unpublished Manuscript. University of Cambridge.

Bennett, K.D., Whittington, G., Edwards, K.J., 1994. Recent plant nomenclatural changes and pollen morphology in the British Isles. Quat. Newsl. 73, 1–6.

Blackmore, S., Steinmann, J.A.J., Hoen, P.P., Punt, W., 2003. The Northwest european Pollen Flora, 65: betulaceae and Corylaceae. Rev. Palaeobot. Palynol. 123, 71–98. https://doi.org/10.1016/S0034-6667(02)00156-2.

Bøtter-Jensen, L., Mejdahl, V., Murray, A.S., 1999. New light on OSL. Quat. Sci. Rev. 18, 303–310. https://doi.org/10.1016/S0277-3791(98)00063-8.

Bridgland, D.R., Preece, R.C., Roe, H.M., Tipping, R.M., Coope, G.R., Field, M.H., Robinson, J.E., Schreve, D.C., Crowe, K., 2001. Middle Pleistocene interglacial deposits at Barling, Essex, England: evidence for a longer chronology for the Thames terrace sequence. J. Quat. Sci. 16, 813–840. https://doi.org/10.1002/jqs.617.

Bronk Ramsey, C., 2009. Bayesian analysis of radiocarbon dates. Radiocarbon 51, 337–360. https://doi.org/10.1017/S0033822200033865.

Bronk Ramsey, C., 2021. OxCal v.4.4.4 [software]. URL: https://c14.arch.ox.ac.uk/oxcal.html.

Bronk Ramsey, Christopher, 2008. Deposition models for chronological records. Quaternary Science Reviews 27 (1-2), 42–60. https://doi.org/10.1016/j.quascirev.2007.01.019. https://linkinghub.elsevier.com/retrieve/pii/S0277379107003617.

Bryant, I.D., Holyoak, D.T., Moseley, K.A., 1983. Late Pleistocene deposits at Brimpton, Berkshire, England. PGA (Proc. Geol. Assoc.) 94 (4), 321–343. https://doi.org/10.1016/S0016-7878(83)80015-7.

Busschers, F.S., 2012. Radiocarbon ghostdates from southern North Sea marine shells. Quat. Int. 279–280, 76. https://doi.org/10.1016/j.quaint.2012.07.333.

Busschers, F.S., Wesselingh, F., Kars, R., Versluijs-Helder, M., Wallinga, J., Bosch, J., Timmner, J., Nierop, K., Meijer, T., Bunnik, F., Wolf, H., 2014. Radiocarbon dating of late Pleistocene marine shells from the Southern North Sea. Radiocarbon 56, 1151–1166. https://doi.org/10.2458/56.16505.

Buylaert, J.P., Vandenberghe, D., Murray, A.S., Huot, S., Corte, F.D., den Haute, P.V., 2007. Luminescence dating of old (>70 ka) Chinese loess: a comparison of single-aliquot OSL and IRSL techniques. Quat. Geochronol. 2, 9–14. https://doi.org/10.1016/j.quageo.2006.05.028.

Bynoe, R., Grant, M., Dix, J., 2022. Strategic Support for Marine Development Management: palaeolithic archaeology and landscape reconstruction offshore. Historic England Research Report 90/2022. https://historicengland.org.uk/research/results/reports/90-2022.

Calarossi, D., Duller, G.A.T., Roberts, H.M., Tooth, S., Lyons, R., 2015. Comparison of paired quartz OSL and feldspar post-IR IRSL dose distributions in poorly bleached fluvial sediments from South Africa. Quat. Geochronol. 30, 233–238. https://doi.org/10.1016/j.quageo.2015.02.015.

Cameron, N., 2018. Diatom assessment of samples from Hornsea Offshore Wind farm (Offshore cores). In: Heamagi, C. (Ed.), Hornsea Project One Offshore Wind Farm Stage 3 Geoarchaeological Assessment Report. Report No. 2702051A. Maritime Archaeology Ltd, Southampton, pp. 31–35. https://doi.org/10.5284/1051479.

Cameron, T.D.J., Crosby, A., Balson, P.S., Jeffrey, D.H., Lott, G.K., Bulat, J., Harrison, D. J., 1992. The geology of the southern North Sea. British Geological Survey. https://pubs.bgs.ac.uk/publications.html?pubID=B01848.

Caselitz, B., McKay, A., Widmaier, M., Oukili, J., Davies, D., Pernin, N., 2025. Harnessing 3D ultra-high-resolution seismic technology for offshore wind farm development: advancements, challenges, and future prospects. Lead. Edge 44 (3), 158–236. https://doi.org/10.1190/tle44030170.1.

Cheng, T., Zhang, D., Zhao, H., Yang, S., Li, B., 2022. Bleachability of pIRIR signal from single-grain K-feldspar. Quat. Geochronol. 71, 101321. https://doi.org/10.1016/j.quageo.2022.101321.

Clark, C.D., Ely, J.C., Hindmarsh, R.C.A., Bradley, S., Ignéczi, A., Fabel, D., Cofaigh, C.O., Chiverrell, R.C., Scourse, J., Benetti, S., Bradwell, T., Evans, D.J.A., Roberts, D.H., Burke, M., Callard, S.L., Medialdea, A., Saher, M., Small, D., Smedley, R.K., Gasson, E., Gregoire, L., Gandy, N., Hughes, A.L.C., Ballantyne, C., Bateman, M.D., Bigg, G.R., Doole, J., Dove, D., Duller, G.A.T., Jenkins, G.T.H., Livingstone, S.L., McCarron, S., Moreton, S., Pollard, D., Praeg, D., Sejrup, H.P., Van Landeghem, K.J. J., Wilson, P., 2022. Growth and retreat of the last British–Irish Ice Sheet, 31 000 to 15 000 years ago: the BRITICE-CHRONO reconstruction. Boreas 51, 699–876. https://doi.org/10.1111/bor.12594.

Cohen, K., Westley, K., Erkens, G., Hijma, M., Weerts, H., 2017. The North Sea. In: Flemming, N., Harff, J., Moura, D., Burgess, A., Bailey, G. (Eds.), Submerged Landscapes of the European Continental Shelf: Quaternary Palaeoenvironments. John Wiley & Sons, Chichester, pp. 147–186. https://doi.org/10.1002/9781118927823.ch7.

Cohen, K.M., Cartelle, V., Barnett, R., Busschers, F.S., Barlow, N.L.M., 2022. Last Interglacial sea-level data points from Northwest Europe. Earth Syst. Sci. Data 14 (6), 2895–2937. https://doi.org/10.5194/essd-14-2895-2022.

Cotterill, C.J., Phillips, E., James, L., Forsberg, C.F., Tjelta, T.I., Carter, G., Dove, D., 2017. The evolution of the Dogger Bank, North Sea: a complex history of terrestrial, glacial and marine environmental change. Quat. Sci. Rev. 171, 136–153. https://doi.org/10.1016/j.quascirev.2017.07.006.

Coxon, P., 1985. A hoxnian interglacial site at Athelington, Suffolk. New Phytol. 99 (4), 611–621. https://doi.org/10.1111/j.1469-8137.1985.tb03687.x.

Creveling, J.R., Mitrovica, J.X., Clark, P.U., Waelbroeck, C., Pico, T., 2017. Predicted bounds on peak global mean sea level during marine isotope stages 5a and 5c. Quat. Sci. Rev. 163, 193–208. https://doi.org/10.1016/j.quascirev.2017.03.003.

Dakin, N., Dove, D., Lee, J., MacDonald, C., 2026. The Shallow Subsurface Geology of the Southern North Sea (UK): an Updated Assessment Using Data from Offshore Wind Farms. British Geological Survey Open Report. OR/26/0055. 84pp. https://nora.nerc.ac.uk/id/eprint/541271.

Davtian, N., Bard, E., 2023. Composite Greenland atmospheric temperature record from the GISP2, NGRIP, and NEEM ice cores. PANGAEA. https://doi.org/10.1594/PANGAEA.957135.

Dix, J., Sturt, F., 2013. Marine geoarchaeology and investigative methodologies. In: Ransley, J., Sturt, F., Dix, J., Adams, J., Blue, L. (Eds.), People and the Sea: a Maritime Archaeological Research Agenda for England, vol.171. CBA Research Report, pp. 1–9. https://doi.org/10.5284/1081826.

Dove, D., Evans, D.J.A., Lee, J.R., Roberts, D.H., Tappin, D.R., Mellett, C.L., Long, D., Callard, S.L., 2017. Phased occupation and retreat of the last British–Irish Ice Sheet in the southern North Sea; geomorphic and seismostratigraphic evidence of a dynamic ice lobe. Quat. Sci. Rev. 1663, 114–134. https://doi.org/10.1016/j.quascirev.2017.03.006.

Duller, G.A.T., 2003. Distinguishing quartz and feldspar in single grain luminescence measurements. Radiat. Meas. 37, 161–165. https://doi.org/10.1016/S1350-4487(02)00170-1.

Duller, G.A.T., 2008. Luminescence Dating: Guidelines on using luminescence dating in archaeology. English Heritage.

Duller, G.A.T., 2015. The Analyst software package for luminescence data: overview and recent improvements. Ancient TL 33, 35–42. https://hdl.handle.net/2160/29712.

Duller, G.A.T., 2025. Luminescence dating. In: Grant, M., Marshall, P. (Eds.), Scientific Dating of Pleistocene Sites: Guidelines for Best Practice. Historic England Advice and Guidance HEAG325. Historic England, London, pp. 35–40. Accessible at: https://historicengland.org.uk/images-books/publications/scientific-dating-pleistocene-sites/.

Duller, G.A.T., Bøtter-Jensen, L., Murray, A.S., 2003. Combining infrared- and green-laser stimulation sources in single-grain luminescence measurements of feldspar and quartz. Radiat. Meas. 37, 543–550. https://doi.org/10.1016/S1350-4487(03)00050-7.

Eaton, S.J., Hodgson, D.M., Barlow, N.L.M., Mortimer, E.E.J., Mellett, C.L., 2020. Palaeogeographical changes in response to glacial–interglacial cycles, as recorded in Middle and Late Pleistocene seismic stratigraphy, southern North Sea. J. Quat. Sci. 35 (6), 760–775. https://doi.org/10.1002/jqs.3230.

Ehlers, J., Wingfield, R., 1991. The extension of the late Weichselian/late Devensian ice sheets in the North Sea basin. J. Quat. Sci. 6, 313–326. https://doi.org/10.1111/j.1502-3885.1994.tb00581.x.

Ekman, S.R., Scourse, J.D., 1993. Early and Middle Pleistocene pollen stratigraphy from British Geological Survey borehole 81/26, Fladen Ground, central North Sea. Rev. Palaeobot. Palynol. 79, 285–295. https://doi.org/10.1016/0034-6667(93)90027-R.

Finsinger, W., Tinner, W., 2020. New insights on stomata analysis of European conifers 65 years after the pioneering study of werner Trautmann (1953). Veg. Hist. Archaeobotany 29, 393–406. https://doi.org/10.1007/s00334-019-00754-1.

Firth, A., 2013. Marine Spatial Planning and the Historic Environment. Fjordr. Report No. 16030, Accessible at: https://historicengland.org.uk/images-books/publications/marine-spatial-planning-historic-environment/.

Fisher, M.J., Funnell, B.M., West, R.G., 1969. Foraminifera and pollen from a marine interglacial deposit in the western North Sea. Proceedings of the Yorkshire Geological Society 37 (3), 311–320. https://doi.org/10.1144/pygs.37.3.311. https://www.lyellcollection.org/doi/10.1144/pygs.37.3.311. (Accessed 6 June 2022).

Forden, S.J., 2015. British Palaeoclimates and Palaeoenvironments During the Hoxnian Interglacial (Marine Isotope Stage 11). Unpublished PhD Thesis, Queen Mary University of London. Accessible at: https://qmro.qmul.ac.uk/xmlui/handle/123456789/12830.

Fugro, 2013. Hornsea offshore windfarm cable route Survey. Geotechnical investigation. Final factual report. Fugro Alluvial Offshore Ltd. Report Number: 120549-7 (02).

Gaffney, V., Fitch, S., 2022. Europe's lost frontiers. Archaeopress 1. Oxford. https://www.archaeopress.com/Archaeopress/Products/9781803272689.

Gaffney, V., Fitch, S., Smith, D., 2009. Europe's Lost World. the Rediscovery of Doggerland. Research Report No 160. Council for British Archaeology.

Gaffney, V., Thomson, K., Fitch, S., 2007. Mapping Doggerland: the Mesolithic Landscapes of the Southern North Sea. Archaeopress, Oxford.

Galbraith, R.F., Roberts, R.G., Laslett, G.M., Yoshida, H., Olley, J.M., 1999. Optical dating of single and multiple grains of quartz from Jinmium rock shelter (northern Australia): part I, experimental design and statistical models. Archaeometry 41, 339–364. https://doi.org/10.1111/j.1475-4754.1999.tb00987.x.

Gardline, 2015. Triton Knoll offshore wind Farm limited. Triton Knoll Offshore Wind Farm, UHR Survey results. Gardline Report Ref 10567.2. Dataset and report available from: the Marine Data Exchange: https://www.marinedataexchange.co.

uk/details/TCE-2149/2015-gardline-geosurvey-limited-triton-knoll-offshore-wind-farm-geophysical-survey.
Gatliff, R.W., Richards, P.C., Smith, K., Graham, C.C., McCormac, M., Smith, N.J.P., Long, D., Cameron, T.D.J., Evans, D., Stevenson, A.G., Bulat, J., Ritchie, J.D., 1994. United Kingdom Offshore Regional Report: the Geology of the Central North Sea. HMSO for the British Geological Survey, London. Accessible at: https://webapps.bgs.ac.uk/Memoirs/docs/B01846.html.
Gibbard, P.L., Bateman, M.D., Leathard, J., West, R.G., 2021. Luminescence dating of a late Middle Pleistocene glacial advance in eastern England. Neth. J. Geosci. 100, e18. https://doi.org/10.1017/njg.2021.13.
Gibbard, P.L., West, R.G., Turner, C., 2013. The Bytham river reconsidered. Quat. Int. 292, 15–32. https://doi.org/10.1016/j.quaint.2012.08.2053.
Graham, A., 1971. British Prosobranchs. Academic Press/The Linnean Society, London.
Graham, A.G.C., Stoker, M.S., Lonergan, L., Bradwell, T., Stewart, M.A., 2011. The Pleistocene glaciations of the North Sea basin. In: Ehlers, J., Gibbard, P.L. (Eds.), Quaternary Glaciations – Extent and Chronology, second ed. Elsevier, Amsterdam, pp. 261–278. https://doi.org/10.1016/B978-0-444-53447-7.00021-0.
Grant, M., Hill, T., Evans, S., Law, M., 2024. Coastal lagoonal evolution within the early Holocene Humber Estuary, eastern England. J. Quat. Sci. 39 (2), 234–247. https://doi.org/10.1002/jqs.3585.
Grant, M., Marshall, P., 2025a. Scientific Dating of Pleistocene Sites: guidelines for best practice. Historic England advice and guidance HEAG325. Historic England, London. Accessible at: https://historicengland.org.uk/images-books/publications/scientific-dating-pleistocene-sites/.
Grant, M., Marshall, P., 2025b. Great Pan Farm: a refined chronology for Late Middle Palaeolithic re-occupation in Britain. Quat. Int. https://doi.org/10.1016/j.quaint.2025.110033 (in press).
Gribble, J., Leather, S., 2011. Offshore geotechnical investigations and historic environment analysis: guidance for the renewable energy sector. Commissioned by COWRIE Ltd (project reference GEOARCH-09). Accessible at: https://www.historicenvironment.scot/media/2376/2011-01-offshore-geotechnical-investigations-and-historic-environment-analysis-guidance-for-the-renewable-energy-sector.pdf.
Hayward, Bruce W., Holzmann, Maria, Grenfell, Hugh R., Pawlowski, Jan, Triggs, Chris M., 2004. Morphological distinction of molecular types in Ammonia – towards a taxonomic revision of the world's most commonly misidentified foraminifera. Marine Micropaleontology 50 (3-4), 237–271. https://doi.org/10.1016/s0377-8398(03)00074-4. https://linkinghub.elsevier.com/retrieve/pii/S0377839803000744.
Heamagi, C., 2018. Hornsea Project One Offshore Wind Farm Stage 3 Geoarchaeological Assessment Report. Maritime Archaeology Ltd, Southampton. https://doi.org/10.5284/1051479. Report No. 2702051A.
Heaton, T.J., Köhler, P., Butzin, M., Bard, E., Reimer, R.W., Austin, W.E.N., Bronk Ramsey, C., Grootes, P.M., Hughen, K.A., Kromer, B., Reimer, P.J., Adkins, J., Burke, A., Cook, M.S., Olsen, J., Skinner, L.C., 2020. Marine20 – the marine radiocarbon age calibration Curve (0-55,000 cal. BP). Radiocarbon 62, 779–820. https://doi.org/10.1017/RDC.2020.68.
Hijma, M.P., Cohen, K.M., Roebroeks, W., Westerhoff, W.E., Busschers, F.S., 2012. Pleistocene Rhine–Thames landscapes: geological background for hominin occupation of the southern North Sea region. J. Quat. Sci. 27 (1), 17–39. https://doi.org/10.1002/jqs.1549.
Historic England, 2011. Environmental Archaeology. A Guide to the Theory and Practice of Methods, from Sampling and Recovery to Post-excavation, second ed. English Heritage. Accessible at: https://historicengland.org.uk/images-books/publications/environmental-archaeology-2nd/.
Historic England, 2015. Geoarchaeology: Using Earth Sciences to Understand the Archaeological Record. third edition, English Heritage. Accessible at: https://historicengland.org.uk/images-books/publications/geoarchaeology-earth-sciences-to-understand-archaeological-record/.
Hodgson, J.M., 1997. Soil Survey Field Handbook, third ed. Silsoe: Soil Survey Technical Monograph No. 5.
Holmes, R., 1997. Quaternary stratigraphy: the offshore record. In: Gordon, J.E. (Ed.), Reflections on the Ice Age in Scotland. Scottish Association of Geography Teachers and Scottish Natural Heritage, Glasgow, pp. 72–94.
Huntley, D.J., Lamothe, M., 2001. Ubiquity of anomalous fading in K-feldspars and the measurement and correction for it in optical dating. Can. J. Earth Sci. 38, 1093–1106. https://doi.org/10.1139/e01-013.
Hütt, G., Jaek, I., Tchonka, J., 1988. Optical dating: K-feldspars optical response stimulation spectra. Quaternary Science Reviews 7 (3-4), 381–385. https://doi.org/10.1016/0277-3791(88)90033-9. https://linkinghub.elsevier.com/retrieve/pii/0277379188900339.
Iversen, J., 1958. The bearing of glacial and interglacial epochs on theformation and extinction of plant taxa. Upps. Univ. Årsskrift 6, 210–215.
Jensen, K.A., Knudsen, K.L., 1988. Quaternary foraminiferal stratigraphy in boring 81/29 from the central North Sea. Boreas 17, 273–287. https://doi.org/10.1111/j.1502-3885.1988.tb00957.x.
Jones, D.L., Salter, E., 2017. Archaeological palaeolandscape assessment for marine offshore development using seismic and geotechnical data – the UK experience. In: Offshore Site Investigation Geotechnics 8th International Conference Proceeding, pp. 1315–1322. https://doi.org/10.3723/OSIG17.1315.
Kirkham, J.D., Hogan, K.A., Larter, R.D., Self, E., Games, K., Huuse, M., Stewart, M.A., Ottesen, D., Arnold, N.S., Dowdeswell, J.A., 2021. Tunnel valley infill and genesis revealed by high-resolution 3-D seismic data. Geology 449, 1516–1520. https://doi.org/10.1130/G49048.1.
Kristensen, P., Knudsen, K.L., Sejrup, H.P., 1998. A Middle Pleistocene glacial–interglacial succession in the Inner Silver Pit, southern North Sea: foraminiferal stratigraphy and amino-acid Geochronology. Quat. Sci. Rev. 17, 901–911. https://doi.org/10.1016/S0277-3791(98)00024-9.
Küster, H., 1988. Vom werden einer Kulturlandschaft. Vegetationsgeschichtliche Studien am Auerberg (Südbayern) VHC. Acta Humanoria. Weinheim.
Langdon, C., Scaife, R., 2018. Hornsea (HOW 01) offshore sediment: an assessment of the sub-fossil pollen and spore content. In: Heamagi, C. (Ed.), Hornsea Project One Offshore Wind Farm Stage 3 Geoarchaeological Assessment Report. Report No. 2702051A. Maritime Archaeology Ltd, Southampton, pp. 26–30. https://doi.org/10.5284/1051479.
Li, B., Roberts, R.G., Jacobs, Z., Li, S.-H., 2014. A single-aliquot luminescence dating procedure for K-feldpsar based on the dose-dependent MET-pIRIR signal sensitivity. Quat. Geochronol. 20, 51–64. https://doi.org/10.1016/j.quageo.2013.11.001.
Liénart, C., Cirtwill, A.R., Hedgespeth, M.L., Bradshaw, C., 2022. A sprinkling of gold dust: pine pollen as a carbon source in Baltic Sea coastal food webs. Limnol. Oceanogr. 67 (1), 53–65. https://doi.org/10.1002/lno.11974.
Lisiecki, L.E., Raymo, M.E., 2005. A Pliocene-Pleistocene stack of 57 globally distributed benthic δ18O records. Paleoceanogr. Paleoclimatol. 20, 1. https://doi.org/10.1029/2004PA001071.
Maddy, D., Lewis, S.G., Scaife, R.G., Bowen, D.Q., Coope, G.R., Green, C.P., Hardaker, T., Keen, D.H., Rees-Jones, J., Parfitt, S., Scott, K., 1998. The upper Pleistocene deposits at Cassington, near Oxford England. J. Quat. Sci. 13, 205–231. https://doi.org/10.1002/(SICI)1099-1417(199805/06)13:3%3C205::AID-JQS357%3E3.0.CO;2-N.
Mahan, S., DeWitt, R., 2019. Principles and history of luminescence dating. In: Bateman, M.D. (Ed.), The Handbook of Luminescence Dating. Whittles Publishing, pp. 1–39.
Markey, B.G., Bøtter-Jensen, L., Duller, G.A.T., 1997. A new flexible system for measuring thermally and optically stimulated luminescence. Radiat. Meas. 27, 83–89. https://doi.org/10.1016/s1350-4487(96)00126-6.
Mayer, L.M., Jorgensen, J., Schnitker, D., 1991. Enhancement of diatom frustule dissolution by iron oxides. Mar. Geol. 99 (1–2), 263–266. https://doi.org/10.1016/0025-3227(91)90096-M.
Mejdahl, V., 1979. Thermoluminescence dating: beta-dose attenuation in quartz grains. Archaeometry 21, 61–72. https://doi.org/10.1111/j.1475-4754.1979.tb00241.x.
Mellett, C., 2019a. Norfolk Boreas offshore wind farm. Stage 4 palaeoenvironmental analysis. Wessex Archaeology, Salisbury. Report 117122.01.
Mellett, C., 2019b. Norfolk vanguard Offshore wind farm: stage 4 palaeoenvironmental assessment. Salisbury, wessex archaeology. Report No. 114844.01. https://doi.org/10.5284/1076181.
Merritt, J.W., Auton, C.A., Connell, E.R., Hall, A.M., Peacock, J.D., 2003. Cainozoic Geology and Landscape Evolution of north-east Scotland, vol. 67. Memoir of the British Geological Survey, sheets 66E, 76E, 77, 86E, 87W, 87E, 95, 96W, 96E and 97 (Scotland). Accessible at: https://webapps.bgs.ac.uk/memoirs/docs/B06226.html.
Mitchell, G.F., Penny, L.F., Shotton, F.W., West, R.G., 1973. A correlation of Quaternary deposits in the British Isles. Geological Society of London. Special Report 4.
Moore, P.D., Webb, J.A., Collinson, M.E., 1991. Pollen Analysis, second ed. Blackwell Scientific, Oxford.
MSDS Marine, 2018. Hornsea Project two offshore wind farm: method statement for the collection and retention of geotechnical samples for geoarchaeological assessment. MSDS Marine on behalf of Orsted. Doc. No 3077503B 3077503 Case no. 200-18-0323.
Murray, A.S., Wintle, A.G., 2000. Luminescence dating of quartz using an improved single-aliquot regenerative-dose protocol. Radiat. Meas. 32, 57–73. https://doi.org/10.1016/S1350-4487(99)00253-X.
Murray, A.S., Wintle, A.G., 2003. The single aliquot regenerative dose protocol: potential for improvements in reliability. Radiat. Meas. 37, 377–381. https://doi.org/10.1016/S1350-4487(03)00053-2.
Murray, J., 2006. Ecology and Applications of Benthic Foraminifera. Cambridge University Press, Cambridge.
Murray, J.W., 1973. Distribution and Ecology of Living Benthic Foraminiferids. Heinemann, London.
Murray, J.W., 1979. British Nearshore Foraminiferids. Academic Press/The Linnean Society, London.
Murray, J.W., 1991. Ecology and Palaeoecology of Benthic Foraminifera. Longman, Harlow.
Pawley, S.M., Toms, P., Armitage, S.J., Rose, J., 2010. Quartz luminescence dating of Anglian Stage (MIS 12) fluvial sediments: Comparison of SAR age estimates to the terrace chronology of the Middle Thames valley, UK. Quat. Geochronol. 5 (5), 569–582. https://doi.org/10.1016/j.quageo.2009.09.013.
Peeters, H., Murphy, P., Flemming, N.C., 2009. North Sea prehistory research and management framework (NSPRMF). Amersfoort. Accessible at: https://researchframeworks.org/nsprmf/nsprmf-2009/.
Prescott, J.R., Hutton, J.T., 1994. Cosmic ray contributions to dose rates for luminescence and ESR dating: large depths and long-term time variations. Radiat. Meas. 23, 497–500. https://doi.org/10.1016/1350-4487(94)90086-8.
Prins, L.T., Andresen, K.J., Clausen, O.R., Piotrowski, J.A., 2020. Formation and widening of a North Sea tunnel valley — the impact of slope processes on valley morphology. Geomorphology 368, 107347. https://doi.org/10.1016/j.geomorph.2020.107347.
Rasmussen, S.O., Bigler, M., Blockley, S.P., Blunier, T., Buchardt, S.L., Clausen, H.B., Cvijanovic, I., Dahl-Jensen, D., Johnsen, S.J., Fischer, H., Gkinis, V., Guillevic, M., Hoek, W.Z., Lowe, J.J., Pedro, J.B., Popp, T., Seierstad, I.K., Steffensen, J.P., Svensson, A.M., Vallelonga, P., Vinther, B.M., Walker, M.J.C., Wheatley, J.J., Winstrup, M., 2014. A stratigraphic framework for abrupt climatic changes during the last Glacial period based on three synchronized Greenland ice-core records: refining and extending the INTIMATE event stratigraphy. Quat. Sci. Rev. 106, 14–28. https://doi.org/10.1016/j.quascirev.2014.09.007.
Reimer, P.J., Austin, W.E.N., Bard, E., Bayliss, A., Blackwell, P.G., Bronk Ramsey, C., Butzin, M., Cheng, H., Edwards, R.L., Friedrich, M., Grootes, P.M., Guilderson, T.P.,

Hajdas, I., Heaton, T.J., Hogg, A.G., Hughen, K.A., Kromer, B., Manning, S.W., Muschelar, R., Palmer, J.G., Pearson, C., van der Plicht, J., Reimer, R.W., Richards, D.A., Scott, E.M., Southon, J.R., Turney, C.S.M., Wacker, L., Adolphi, F., Büntgen, U., Capano, M., Fahrni, S.M., Fogtmann-Schultz, A., Friedrich, R., Köhler, P., Kudsk, S., Miyake, F., Olsen, J., Reinig, F., Sakamoto, M., Sookdeo, A., Talamo, S., 2020. The IntCal20 northern hemisphere radiocarbon age calibration curve (0–55,000 kBP). Radiocarbon 62, 725–757. https://doi.org/10.1017/RDC.2020.41.

Rendall, H., Worsley, P., Green, F., Parks, D., 1991. Thermoluminescence dating of the Chelford Interstadial. Earth Planet Sci. Lett. 103 (1–4), 182–189. https://doi.org/10.1016/0012-821X(91)90159-F.

Rex, C.I., Bateman, M.D., Buckland, P.C., Panagiotakopulu, E., Livingstone, S.J., Hardiman, M., Eddey, L., 2023. A revision of the British chronostratigraphy within the last glacialinterglacial cycle based on new evidence from Arclid, Cheshire UK. Quat. Sci. Rev. 299, 107882. https://doi.org/10.1016/j.quascirev.2022.107882.

Richter, Daniel, Richter, Andreas, Dornich, Kay, 2015. *Lexsyg smart* — a luminescence detection system for dosimetry, material research and dating application. Geochronometria 42 (1), 202–209. https://doi.org/10.1515/geochr-2015-0022. https://www.geochronometria.com/-Lexsyg-smart-a-luminescence-detection-system-for-dosimetry-material-research-and,185797,0,2.html. (Accessed 4 December 2015).

Rijsdijk, K.F., Passchier, S., Weerts, H.J.T., Laban, C., van Leeuwen, R.J.W., Ebbing, J.H. J., 2005. Revised Upper Cenozoic stratigraphy of the Dutch sector of the North Sea Basin: towards an integrated lithostratigraphic, seismostratigraphic and allostratigraphic approach. Geol. Mijnbouw 84 (2), 129–146. https://doi.org/10.1017/S0016774600023015.

Roberts, D.H., Evans, D.J.A., Callard, S.L., Clark, C.D., Bateman, M.D., Medialdea, A., Dove, D., Cotterill, C.J., Saher, M., Cofaigh, C.O., Chiverrell, R.C., Moreton, S.G., Fabel, D., Bradwell, T., 2018. Ice marginal dynamics of the last British-Irish ice Sheet in the southern North Sea: ice limits, timing and the influence of the Dogger Bank. Quat. Sci. Rev. 198, 181–207. https://doi.org/10.1016/j.quascirev.2018.08.010.

Roberts, R.G., Jacobs, Z., Li, B., Jankowski, N.R., Cunningham, A.C., Rosenfeld, A.B., 2015. Optical dating in archaeology: thirty years in retrospect and grand challenges for the future. J. Archaeol. Sci. 56, 41–60. https://doi.org/10.1016/j.jas.2015.02.028.

Roe, H.M., Preece, R.C., 2011. Incised palaeo-channels of the late Middle Pleistocene thames: age, origins and implications for fluvial palaeogeography and sea-level reconstruction in the southern North Sea basin. Quat. Sci. Rev. 30 (19–20), 2498–2519. https://doi.org/10.1016/j.quascirev.2011.04.007.

Rose, J., 2009. Early and Middle Pleistocene landscapes of eastern England. PGA (Proc. Geol. Assoc.) 120, 3–33. https://doi.org/10.1016/j.pgeola.2009.05.003.

Russell, J., 2009. Lynn and Inner Dowsing Offshore Windfarms – Geoarchaeological Assessment and Analysis: Final Report (Stages 1-4). Wessex Archaeology. https://doi.org/10.5284/1004513. Report No. 59096.02.

Scourse, J.D., Ansari, M.H., Wingfield, R.T.R., Harland, R., Balson, P.S., 1998. A middle Pleistocene shallow marine interglacial sequence, Inner Silver Pit, southern North Sea: pollen and dinoflagellate cyst stratigraphy and sea-level history. Quat. Sci. Rev. 17 (9–10), 871–900. https://doi.org/10.1016/S0277-3791(98)00023-7.

Scourse, J.D., Austin, W.E.N., Sejrup, H.P., Ansari, M.H., 1999. Foraminiferal isoleucine epimerization determinations from the Nar Valley Clay, Norfolk, UK: implications for Quaternary correlations in the southern North Sea basin. Geol. Mag. 136, 543–560. https://doi.org/10.1017/S0016756899002812.

Sejrup, H.P., Aarseth, I., Ellingsen, K.L., Reither, E., Jansen, E., Løvlie, R., Bent, A., Brigham-Grette, J., Larsen, E., Stoker, M., 1987. Quaternary stratigraphy of the Fladen area, central North Sea: a multidisciplinary study. J. Quat. Sci. 2 (1), 35–58. https://doi.org/10.1002/jqs.3390020105.

Shaw, A., Dobbie, J., Toms, P., Wood, J., 2024. A long chronology for the British Late Middle Palaeolithic: MIS 5–MIS 3 occupation at Great Pan Farm (Isle of Wight, England). Quat. Int. 736–737, 109846. https://doi.org/10.1016/j.quaint.2025.109846.

Smith, A., 2019. HOW02 Windfarm Site: Ground Model Report. Ørsted Unpublished Report.

Stace, C., 2010. New flora of the British Isles, 3rd edition. Cambridge University Press, Cambridge.

Stafford, P.J., 2003. The Northwest European Pollen Flora, 58: Azollaceae. Rev. Palaeobot. Palynol. 123, 9–17. https://doi.org/10.1016/S0034-6667(02)00149-5.

Stanley, E.A., 1966. The problem of reworked pollen and spores in marine sediments. Mar. Geol. 4 (6), 397–408. https://doi.org/10.1016/0025-3227(66)90008-9.

Stoker, M.S., Balson, P.S., Long, D., Tappin, D.R., 2011. An overview of the lithostratigraphical framework for the Quaternary deposits on the United Kingdom continental shelf. British Geological Survey Research Report RR/11/03 48.

Stone, P., McMillan, A.A., Floyd, J.D., Barnes, R.P., Phillips, E.R., 2012. British Regional Geology: South of Scotland, fourth ed. Keyworth, Nottingham: British Geological Survey. Accessible at: https://webapps.bgs.ac.uk/memoirs/docs/B07006.html.

Sturt, F., Dix, J., Grant, M.J., 2017. Industry-linked research: submerged landscapes in English waters. In: Bailey, G.N., Harff, J., Sakellariou, D. (Eds.), Under the Sea: Archaeology and Palaeolandscapes of the Continental Shelf. Coastal Research Library, vol. 20. Springer, pp. 425–436. https://doi.org/10.1007/978-3-319-53160-1_28.

Tappin, D.R., Pearce, B., Fitch, S., Dove, D., Gearey, B., Hill, J.M., Chambers, C., Bates, R., Pinnion, J., Diaz Doce, D., Green, M., Gallyot, J., Georgiou, L., Brutto, D., Marzialetti, S., Hopla, E., Ramsay, E., Fielding, H., 2011. The Humber regional environmental characterisation. British Geological Survey Open Report OR/10/54.

Thomas, G.N., 2001. Late Middle Pleistocene pollen biostratigraphy in Britain: pitfalls and possibilities in the separation of interglacial sequences. Quat. Sci. Rev. 20 (16–17), 1621–1630. https://doi.org/10.1016/S0277-3791(01)00026-9.

Thompson, S., Creveling, J., 2021. A global database of marine isotope substage 5a and 5c marine terraces and paleoshoreline indicators. Earth Syst. Sci. Data 13 (7), 3467–3490. https://doi.org/10.5194/essd-13-3467-2021.

Thomsen, K.J., Murray, A.S., Jain, M., Bøtter-Jensen, L., 2008. Laboratory fading rates of various luminescence signals from feldspar-rich sediment extracts. Radiat. Meas. 43, 1474–1486. https://doi.org/10.1016/j.radmeas.2008.06.002.

Toms, P., Wood, J.C., 2019a. Paired Quartz & K-Feldspar Optical dating of sediments: triton Knoll Borehole (26.05-26.90 m), UK. In: Brown, A., Mellett, C. (Eds.), *Triton knoll Offshore Wind Farm and Export Cable Corridor Stage 3 Palaeoenvironmental Assessment*. Wessex Archaeology. https://doi.org/10.5284/1111184. Salisbury, Report 70076.08.

Toms, P., Wood, J.C., 2019b. Optical dating of sediments: Vanguard Offshore Windfarm. In: Mellett, C. (Ed.), Norfolk Vanguard Offshore Wind Farm. Stage 4 Palaeoenvioronmental Analysis. Wessex Archaeology, Salisbury. https://doi.org/10.5284/1076181. Report 114844.01.

Toms, P., Wood, J.C., 2019c. Optical dating of sediments: Boreas Offshore Windfarm. In: Mellett, C. (Ed.), Norfolk Boreas Offshore Wind Farm. Stage 4 Palaeoenvioronmental Analysis. Wessex Archaeology, Salisbury. Report 117122.01 10.5284/107605910.5284/1111184.

Traverse, A., Ginsberg, R.N., 1966. Palynology of the surface sediments of the Great Bahama Bank, as related to water movement and sedimentation. Mar. Geol. 4, 417–459. https://doi.org/10.1016/0025-3227(66)90010-7.

Turner, C., 1970. The middle Pleistocene deposits at marks Tey, essex. Phil. Trans. Biol. Sci. 257, 373–437. https://doi.org/10.1098/rstb.1970.0029.

Tye, G.J., Candy, S.L., Coxon, P., Palmer, A., McClymont, E.L., Schreve, D.C., 2016. The δ18O stratigraphy of the Hoxnian lacustrine sequence at Marks Tey, Essex, UK: implications for the climatic structure of MIS 11 in Britain. J. Quat. Sci. 31, 75–92. https://doi.org/10.1002/jqs.2840.

Tzedakis, P.C., Andrieu, V., de Beaulieu, J.-L., Birks, H.J.B., Crowhurst, S., Follieri, M., Hooghiemstra, H., Magri, D., Reille, M., Sadori, L., Shackleton, N.J., Wijmstra, T.A., 2001. Establishing a terrestrial chronological framework as a basis for biostratigraphical comparisons. Quat. Sci. Rev. 20, 1583–1592. https://doi.org/10.1016/S0277-3791(01)00025-7.

UK Marine Policy Statement, 2011. UK Marine Policy Statement. https://www.gov.uk/government/publications/uk-marine-policy-statement published by the Department for Environment, Food & Rural Affairs, 30 September 2011, last updated 22 September 2020.

Waajen, I.M., Busschers, F.S., Donders, T.H., van Heteren, S., Plets, R., Wallinga, J., Hennekam, R., Reichart, G.-J., Kinnaird, T., Wagner-Cremer, F., 2024. Late MIS5a in the southern North Sea: new chronostratigraphic insights from the Brown Bank Formation. J. Quat. Sci. 39 (3), 408–420. https://doi.org/10.1002/jqs.3592.

Waajen-Labee, I., Plets, R., Cartelle, V., Cuperus, M., Donders, T., van Heteren, S., Mestdagh, T., Wagner-Cremer, F., Wallinga, J., Wesselingh, F., Busschers, F., 2025. Sedimentary architecture of the Brown Bank Formation (Dutch sector of the North Sea) reveals consecutive shallow marine depositional phases during the MIS 5-4 transition. Quat. Sci. Rev. 365, 109442. https://doi.org/10.1016/j.quascirev.2025.109442.

Ward, G.K., Wilson, S.R., 1978. Procedures for comparing and combining radiocarbon age determinations: a critique. Archaeometry 20 (1), 19–31. https://doi.org/10.1111/j.1475-4754.1978.tb00208.x.

Wessex Archaeology, 2013. Round 3 Hornsea Offshore Windfarm Subzone 1 and Export Cable Route: stage 1 and 2 Geoarchaeological Assessment. Report No. 87151.03. Wessex Archaeology, Salisbury. https://doi.org/10.5284/1023470.

West, R., 1970. Pollen zones in the Pleistocene of Great Britain and their correlation. New Phytol. 69 (4), 1179–1183. https://doi.org/10.1111/j.1469-8137.1970.tb02498.x.

Westley, K., Bailey, G., 2013. The Palaeolithic. In: Ransley, J., Sturt, F., Dix, J., Adams, J., Blue, L. (Eds.), People and the Sea: a Maritime Archaeological Research Agenda for England, vol.171. CBA Research Report, pp. 10–29. https://doi.org/10.5284/1081826.

Whittaker, J.E., 2018. Hornsea Offshore Windfarm, North Sea (how 01): Microfossil assessment of samples from 12 boreholes/vibrocores. In: Heamagi, C. (Ed.), Hornsea Project One Offshore Wind Farm Stage 3 Geoarchaeological Assessment Report. Report No. 2702051A. Maritime Archaeology Ltd, Southampton, pp. 36–40. https://doi.org/10.5284/1051479.

Wintle, A.G., Murray, A.S., 2006. A review of quartz optically stimulated luminescence characteristics and their relevance in single-aliquot regeneration dating protocols. Radiat. Meas. 41, 369–391. https://doi.org/10.1016/j.radmeas.2005.11.001.

Wohlfarth, B., 2013. A Review of Early Weichselian Climate (MIS 5d-a) in Europe. Svensk Käarnbränslehantering, Stockholm. Technical report TR-13-03. https://www.skb.com/publication/2677502/TR-13-02.pdf.

WoRMS Editorial Board, 2025. World register of marine species. Available from: https://www.marinespecies.orgatVLIZ.

Yoon, H.H., Kim, J.C., Yoo, D.-G., Lee, G.-S., Hong, S.-H., 2022. Multi dating approach of long marine core sediments from the south-eastern continental shelf of Korea: comparison of SAR OSL, TT-OSL and pIRIR dates. Quat. Geochronol. 73, 101338. https://doi.org/10.1016/j.quageo.2022.101338.

Zhang, J., Guralnik, B., Tsukamoto, S., Ankjærgaard, C., Reimann, T., 2023. The bleaching limits of IRSL signals at various stimulation temperatures and their potential inference of the pre-burial light exposure duration. Front. Earth Sci. 10, 933131. https://doi.org/10.3389/feart.2022.933131.

Zhang, J., Li, S.-H., 2020. Review of the Post-IR IRSL dating protocols of K-Feldspar. Methods Protoc. 3 (1), 7. https://doi.org/10.3390/mps3010007.

Zimmerman, D.W., 1971. Thermoluminescent dating using fine grains from pottery. Archaeometry 13, 29–52. https://doi.org/10.1111/j.1475-4754.1971.tb00028.x.